CHARACTERIZATION OF HIGH FREQUENCY WAVEGUIDE COMPONENTS USING CST

By

Pushkar Bajirao Kulkarni

A thesis submitted in partial fulfillment of

the requirements for the degree of

Master of Science

(Electrical Engineering)

at the

University of Wisconsin- Madison

2011

ACKNOWLEDGEMENTS

It is a pleasure to thank many people who made this thesis possible.

First and foremost, I would like to express my sincere gratitude to my advisor Professor Roanld J. Vernon for the continuous support during my MS study and research, for his patience, motivation, enthusiasm, and immense knowledge. His guidance with writing the thesis, while doing the research was crucial.

During this work I have collaborated with Bryan Fox and Ungku Fazri for whom I have great regard, and I wish to extend my warm thanks to them. I would also like to thank my other group members as well as my friends, Ben and Andrew for many interesting conversations we had, both technical and personal.

I would like to thank my family for the constant encouragement and love that I have relied on during graduate studies and my stay away from home.

Lastly, I would like to thank the U. S. Department of Energy, which supported this work under contract DE-FG02-85ER52122.

ABSTRACT

This report discusses different waveguide components using a simulation software CST. It includes the characterization of rectangular probes which are used for near-field measurements, and a coupling hole which is equivalent to a circular waveguide in order to measure the amount of power circulating in a travelling wave resonator. It also analyzes radiation from a circular waveguide with a baffle which is excited in the TE_{02} mode which is used in high-power, high frequency applications.

TABLE OF CONTENTS

CHAPTER 1

INTRODUCTION

This report is organized in three chapters which include three different small projects. CST Studio 2009 is used to simulate the structures analyzed in this report.

In near-field measurements, waveguide probes are often use as they are simple, rugged, inexpensive along with other desirable characteristics. In order to do these measurements, the waveguide probe characterization is needed, which is covered in Chapter 2.

The TE_{0n} modes are of interest for high frequency, high power applications because as the frequency increases the metal losses get smaller for these modes. In Chapter 3, one such mode the TE_{02}, is analyzed in a circular waveguide with a baffle, which constitutes a simple launcher.

The fourth chapter contains two parts. Part A deals with the propagation of a Gaussian beam when it propagates in free space. Its power contours as a function of distance are also recorded. They are useful in order to obtain an input signal in the travelling wave resonator in the subsequent part. In Part B a coupling hole, for the travelling wave resonator is analyzed. It will be employed in one of the reflectors of the travelling wave resonator to measure the amount of power circulating inside the resonator.

CHAPTER 2

PROBE CHARACTERIZATION

Many near-field measurements are done using an open-ended, unflanged, rectangular waveguide probe. This is because they are simple, rugged, inexpensive and they have a broad far-field radiation pattern without having nulls in the forward hemisphere over their recommended usable bandwidth. They also have relatively low back radiation. In order to do near-field measurements, it is in general required to know the complex far-field measurements in the forward hemisphere in order to compensate for its response in near-field measurements. Hence, for the frequency of operation, an appropriate rectangular waveguide is chosen and its far-field radiation pattern, gain, and reflection coefficient are measured to complete the near-field measurement procedure [1]. The TE_{10} is the dominant mode in the rectangular waveguide. The simulations are carried out at 110 GHz for which F-band (WR-8) waveguide is used. The simulations are done using Microwave CST Studio 2009. Different designs of the waveguide are simulated and compared in this study. The green circle in all the radiation pattern figures represents the side lobe level, which is the side lobe of the minor lobes with maximum intensity out of all minor lobes located outside the angular width of the main beam.

I – Standard WR-8 Waveguide

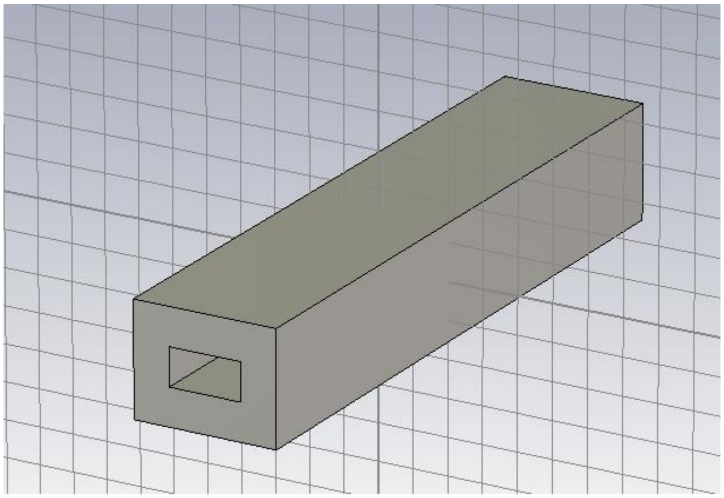

a) Dimensions:-

Inner a = 2.03 mm

Inner b = 1.02 mm

Outer a = 4.06 mm

Outer b = 3.05 mm

b) Gain = e_{rad} * Directivity = 7.75 dB

e_{rad} = -0.0536 dB

Fig. 2-1. Standard (square-cut) WR-8 waveguide.

A standard (square cut) waveguide is shown in Fig.2-1. Significant ripples in the lower part of the E-plane radiation pattern can be seen in Fig. 2-2. As compared to E-plane radiation pattern, the H-plane radiation pattern shown in Fig. 2-3 is smooth. The reflection coefficient (S_{11}) at 110 GHz is about -12.2 dB which means 6.03% of power is reflected at the port. This is shown in Fig. 2-4.

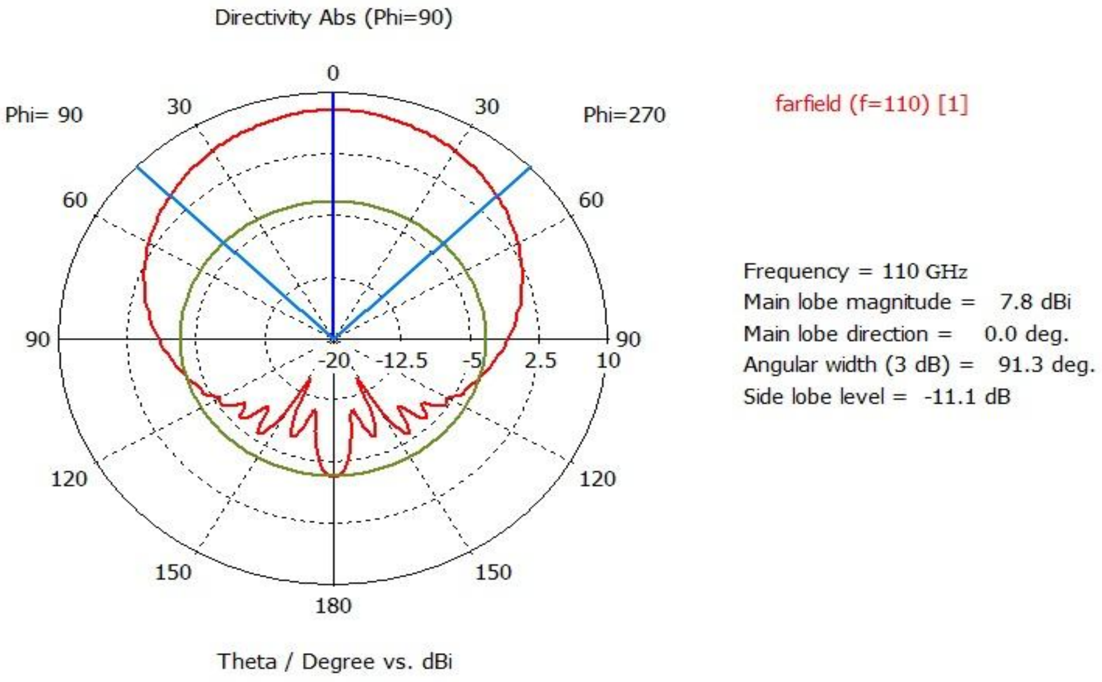

Frequency = 110 GHz
Main lobe magnitude = 7.8 dBi
Main lobe direction = 0.0 deg.
Angular width (3 dB) = 91.3 deg.
Side lobe level = -11.1 dB

Fig. 2-2. E-Plane radiation pattern of a standard (square-cut) WR-8 waveguide.

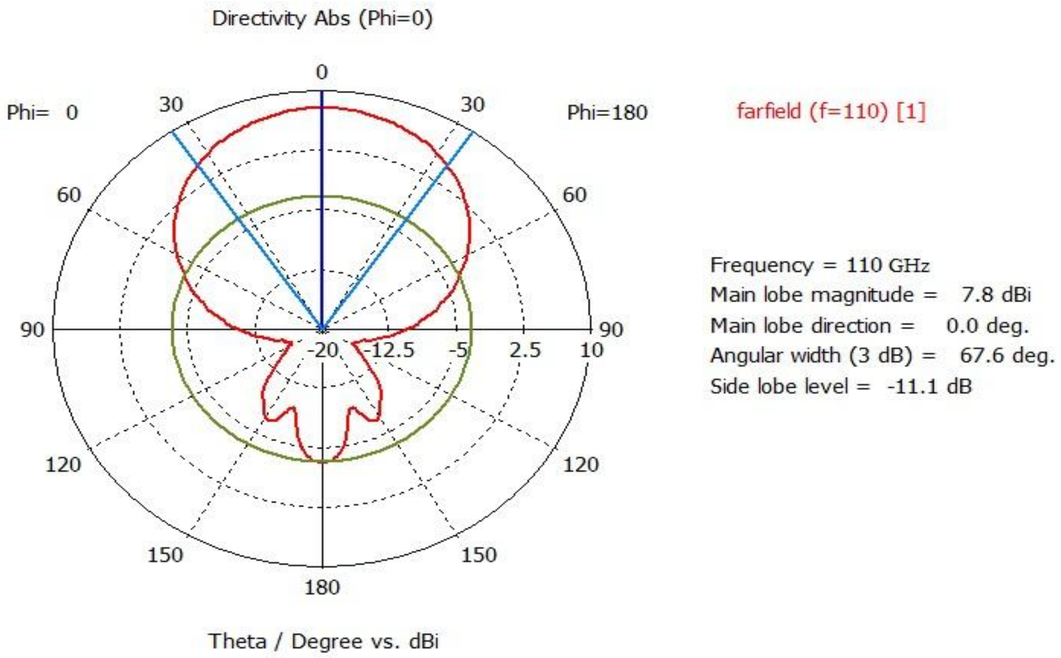

Frequency = 110 GHz
Main lobe magnitude = 7.8 dBi
Main lobe direction = 0.0 deg.
Angular width (3 dB) = 67.6 deg.
Side lobe level = -11.1 dB

Fig. 2-3. H-Plane radiation pattern of a standard (square-cut) WR-8 waveguide.

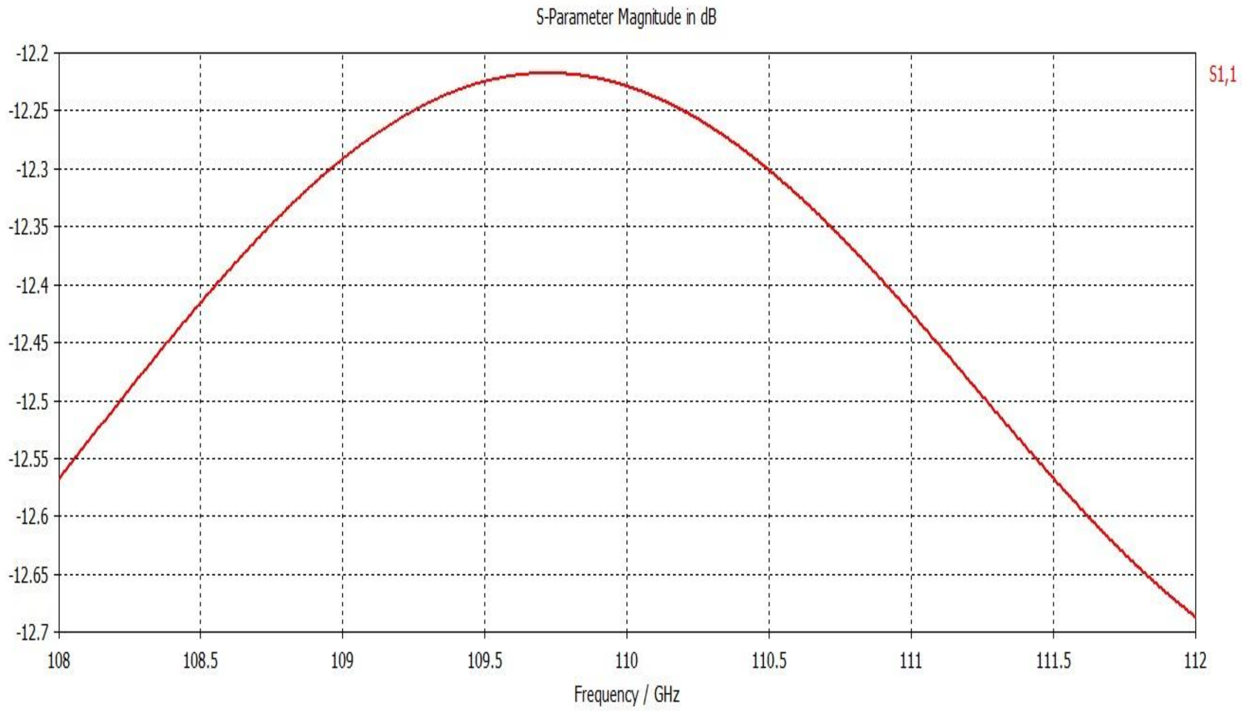

Fig. 2-4. Reflection Coefficient S_{11} (dB) of a standard (square-cut) WR-8 waveguide.

Using a measurement probe in the near-field of the launcher affects the field pattern. This is due to signals scattered from the probe. They are again scattered by the launcher structure. This produces constructive and/or destructive interference at the probe depending on the distance between the probe and the launcher structure. This scattering problem can be minimized by tapering the front end of the measurement probe. Hence different models of the probe are simulated in order to study this effect.

II - Partially Tapered Scanner Probe Model

While studying the tapering effect, inner dimension of the waveguide is kept fixed. In this simulation, the probe is partially tapered as shown in Fig. 2-5. From the E-plane radiation shown in Fig. 2-6, it can be seen that the ripples in the lower part are much less as compared to square cut waveguide shown in Fig. 2-1. Also, the HPBW in E-plane is wider than the square cut model shown above.

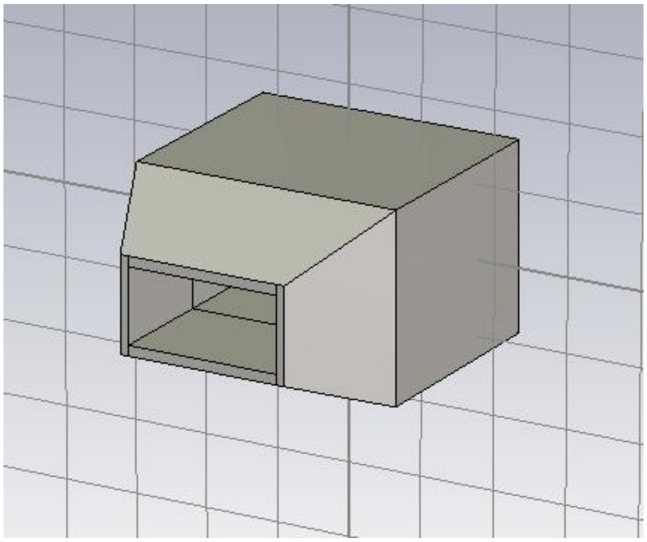

Fig. 2-5. Partially Tapered WR-8 Waveguide.

a) Gain = e_{rad} * Directivity

e_{rad} = -0.0538 dB

Gain = e_{rad} (dB) + Directivity (dB)

Gain = 6.55 dB

b) Average taper length = 2.15 mm

Length of probe (simulated) = 4.5 mm

Length of probe (actual) = 125 mm

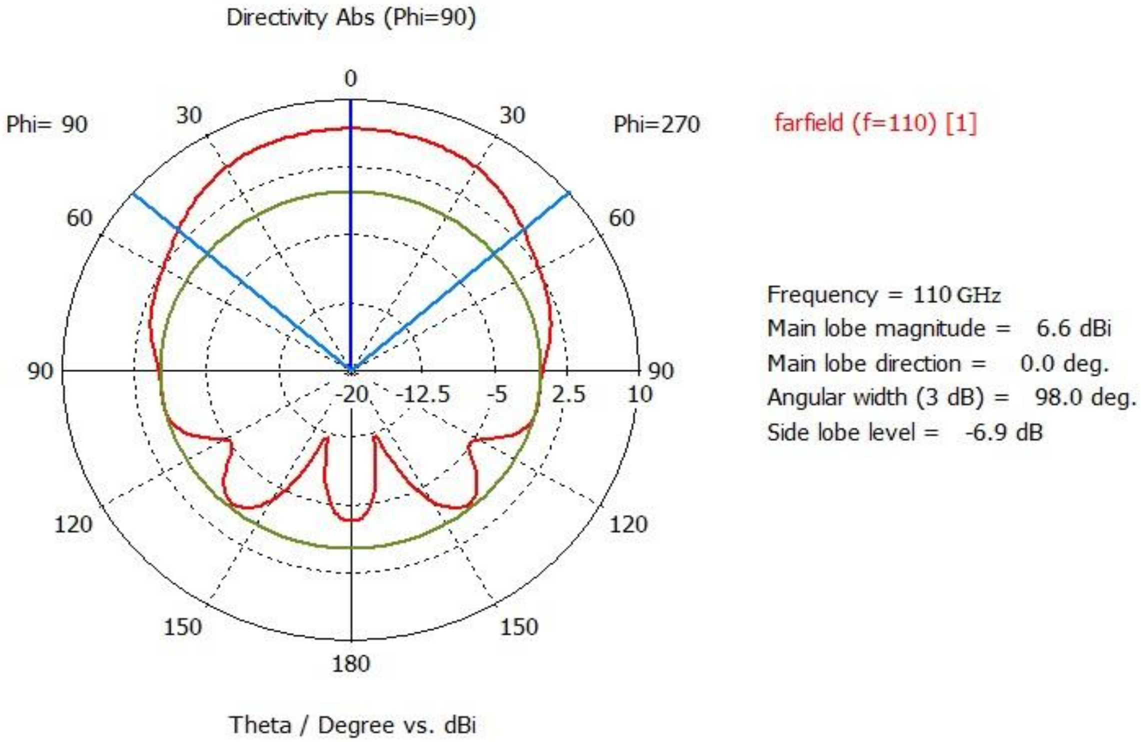

Fig. 2-6. E- Plane radiation pattern of a partially tapered WR-8 waveguide.

H-plane pattern is shown in Fig. 2-7 and it can be seen that it is not much different than the one for the square cut waveguide except the gain. The reflection coefficient (S_{11}) at 110 GHz is around -11.45 dB as shown in Fig. 2-8.

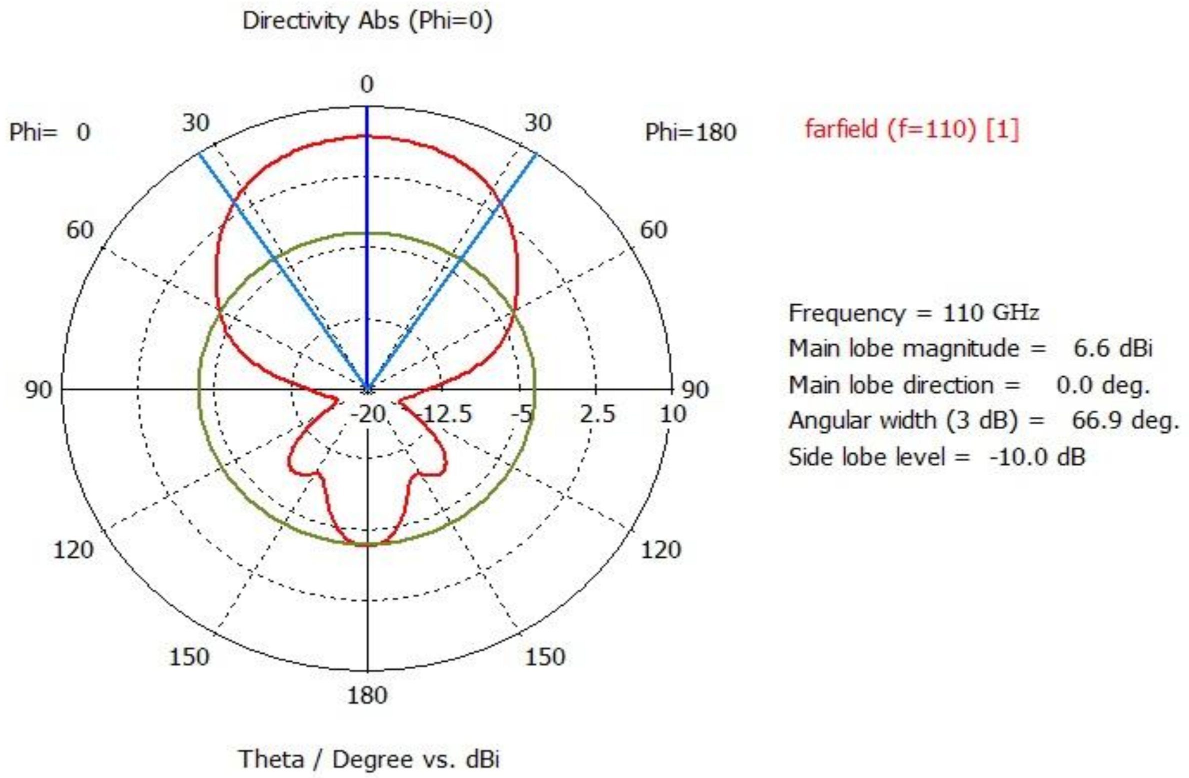

Fig. 2-7. H-Plane radiation pattern of a partially tapered WR-8 waveguide.

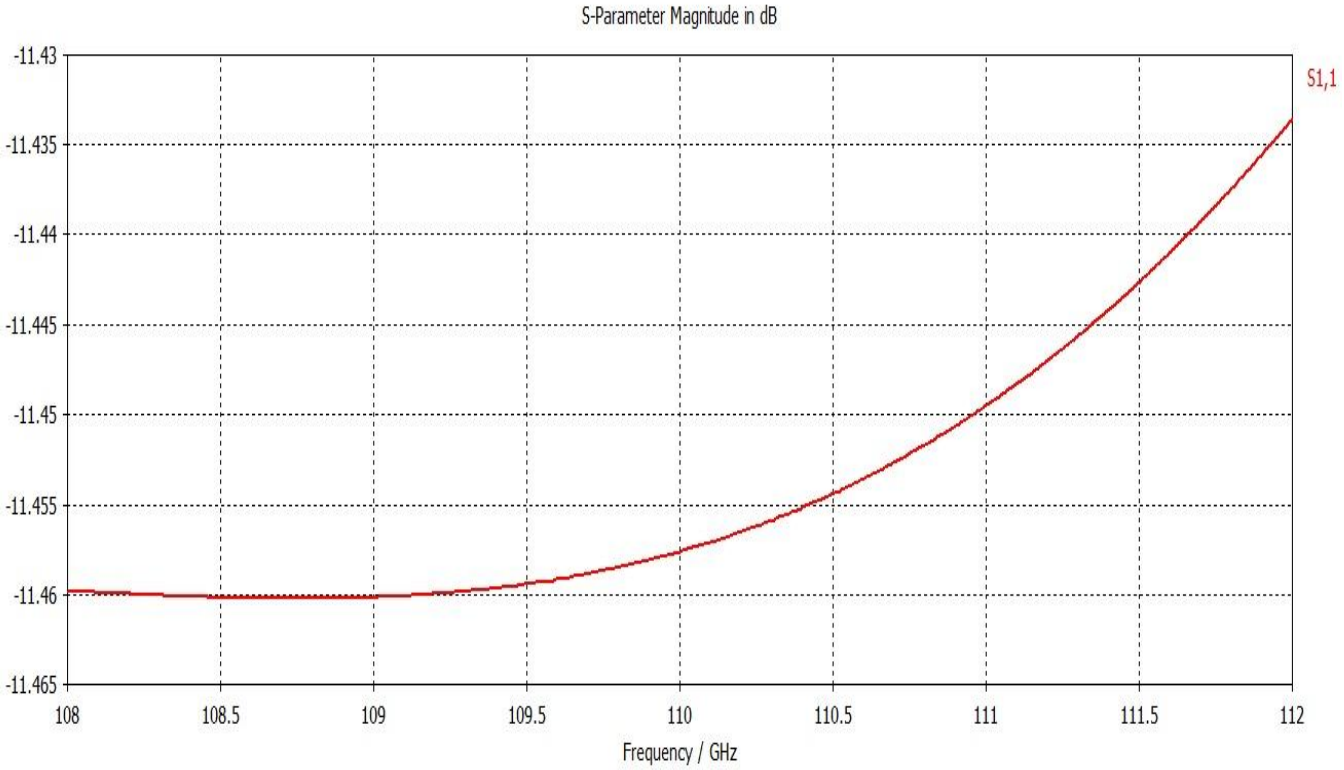

Fig. 2-8. Reflection Coefficient S_{11} (dB) of a partially tapered WR-8 waveguide.

III- F Band short probe

One more model of the probe present in the lab is simulated and its geometry is as shown in Fig. 2-9. Tapering angle in this simulated model is less as compared to model in Fig. 2-5.

a) Gain = e_{rad} * Directivity

e_{rad} = -0.0512 dB

Gain = e_{rad} (dB) + Directivity (dB)

Gain = 7.65 dB

b) Average taper length = 1.75 mm

Length of the probe = 64 mm

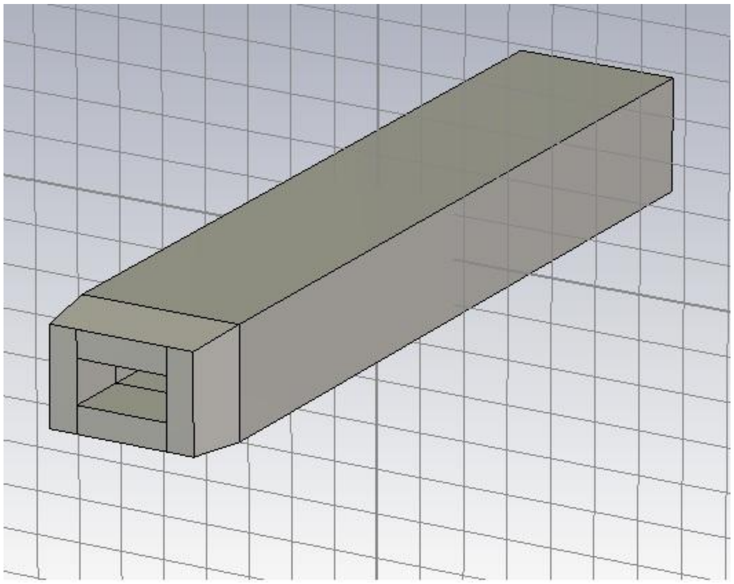

Fig. 2-9. Short probe model of the WR-8 waveguide.

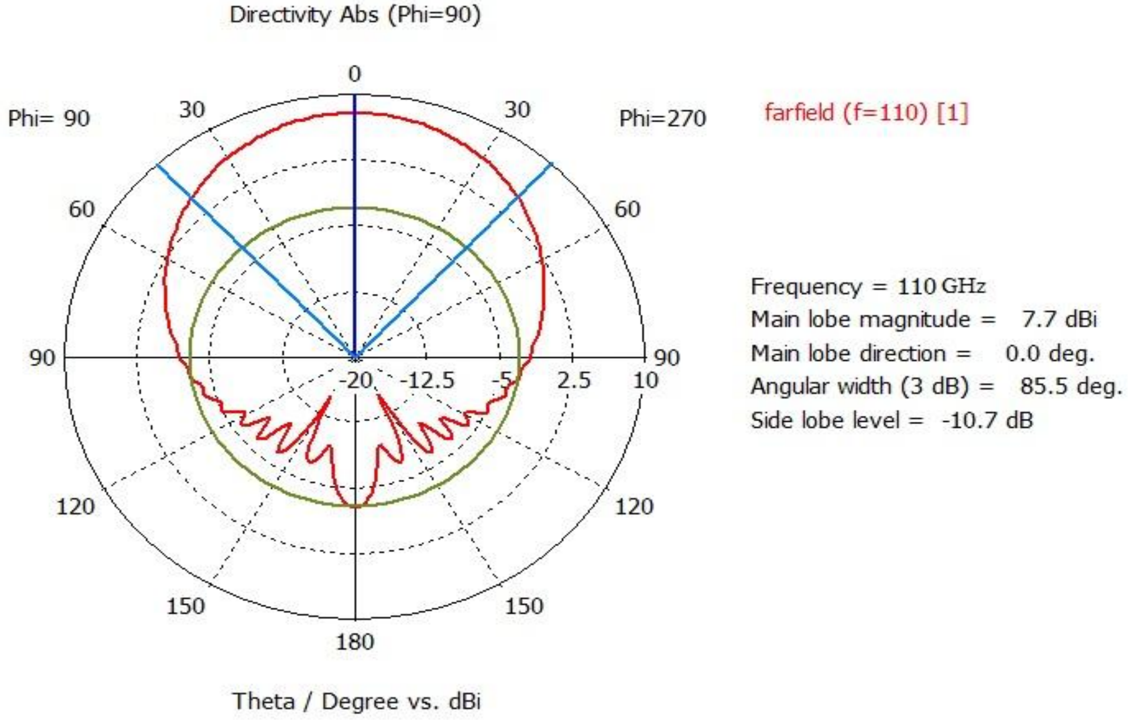

Fig. 2-10. E-Plane radiation pattern of a short probe WR-8 waveguide.

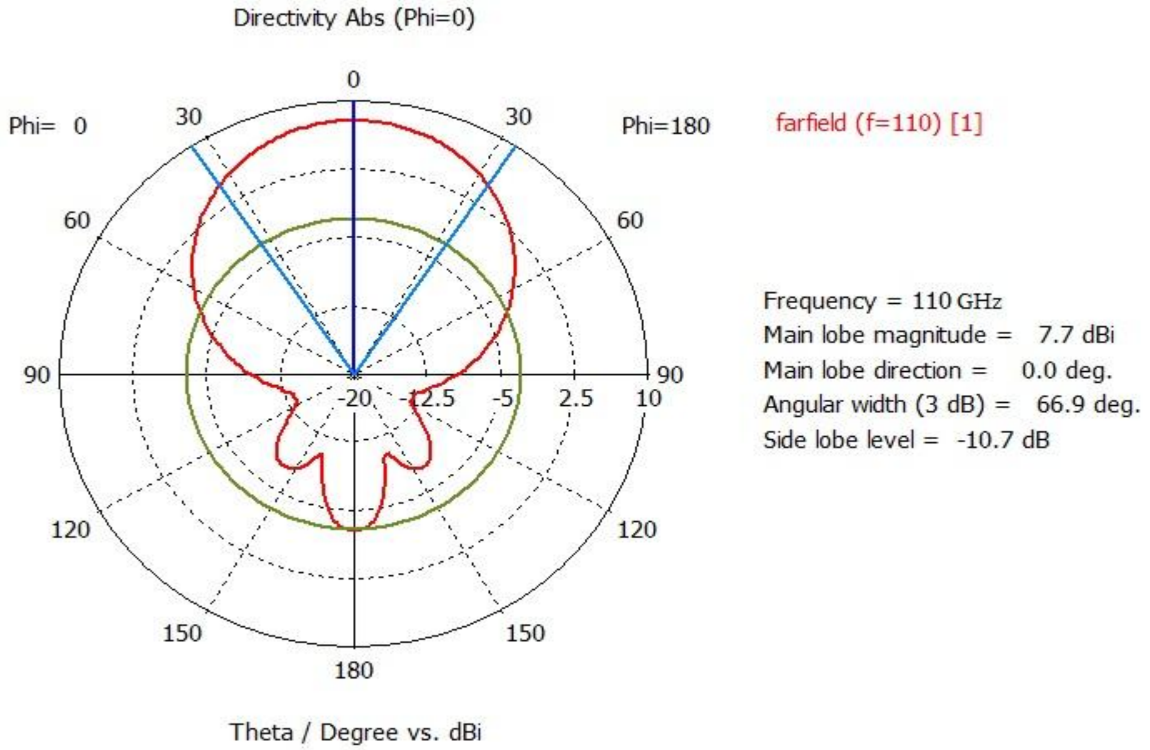

Fig. 2-11. H-Plane radiation pattern of a short probe WR-8 waveguide.

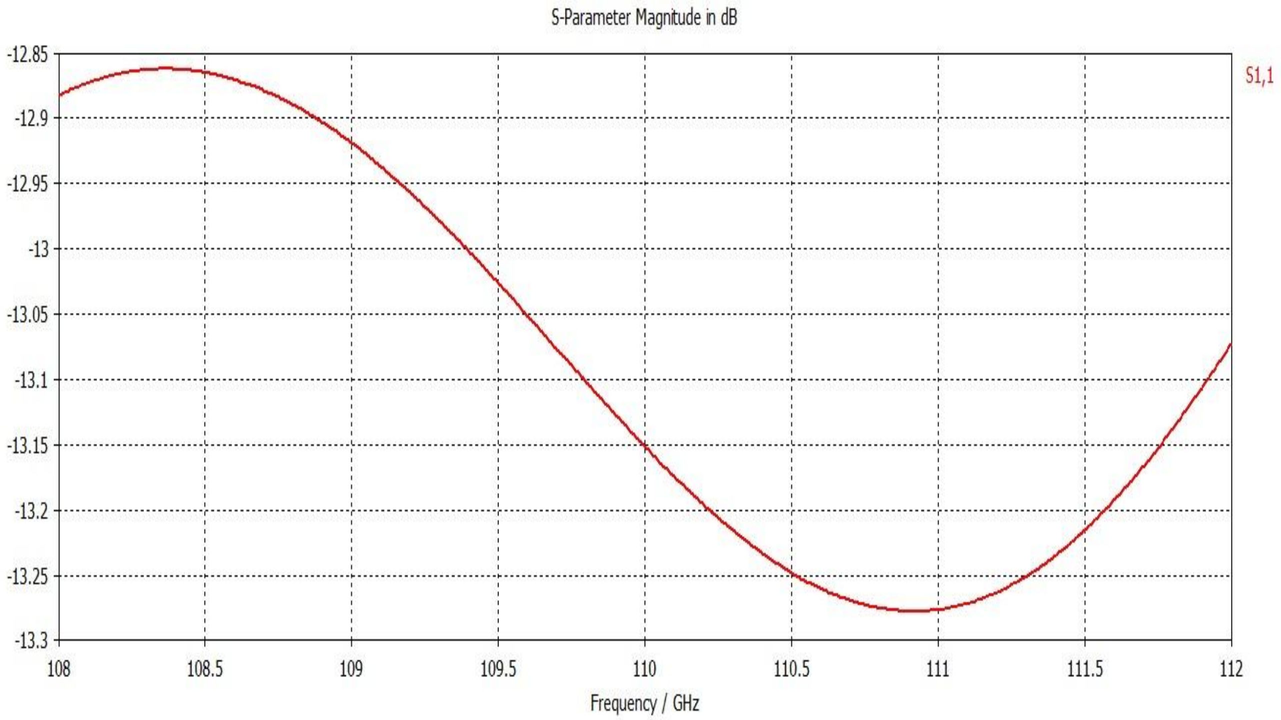

Fig. 2-12. Reflection Coefficient S_{11} (dB) of a short probe WR-8 waveguide.

It can be seen from the E-plane radiation pattern as shown in Fig. 2-10 that the HPBW is 85.5° which is narrower than the models shown in Fig. 2-1 and Fig. 2-5. The H-plane radiation pattern shown in Fig. 2-11 is not much different as compared to the models shown above. The gain of this probe is similar to the square cut WR-8 waveguide shown in Fig.2-1. This model has a reflection coefficient of -13.15 dB at 110 GHz as shown in Fig. 2-12.

IV - Completely Tapered WR-8 Waveguide

It is hard to make a completely tapered probe in practice. But to study its effect, the model shown in Fig. 2-13 is simulated.

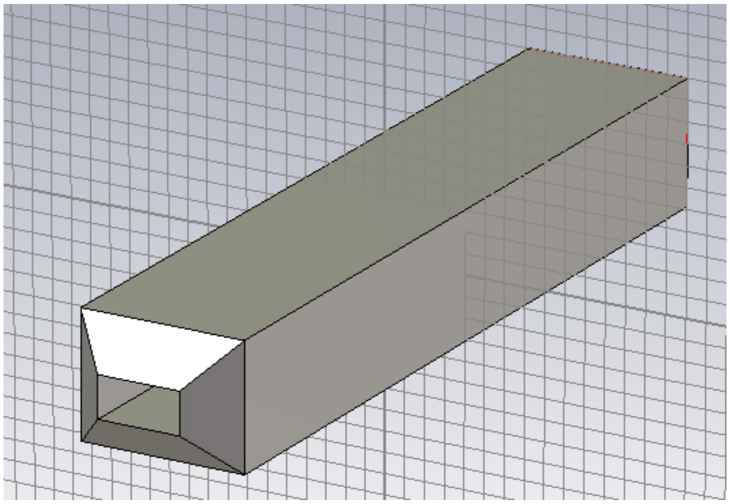

a) Gain = e_{rad} * Directivity

e_{rad} = -0.0523 dB

Gain = e_{rad} (dB) + Directivity (dB)

Gain = 6.35 dB

b) Length of probe = 20.5 mm

Fig. 2-13. Completely Tapered WR-8 waveguide.

It is observed from Fig. 2-14, in the E-plane the HPBW is much wider as compared all the models seen above. However, from Fig. 2-15, in the H-plane this model has a narrower HPBW as compared all others. Even the side lobes in both the planes are increased. The shape of the radiation patterns is similar to other models shown above. Of all the models simulated, this model has least directivity of 6.4 dBi. The reflection coefficient (S11) as a function of frequency is shown in Fig. 2-16. It is observed to be -11.4 dB at 110 GHz.

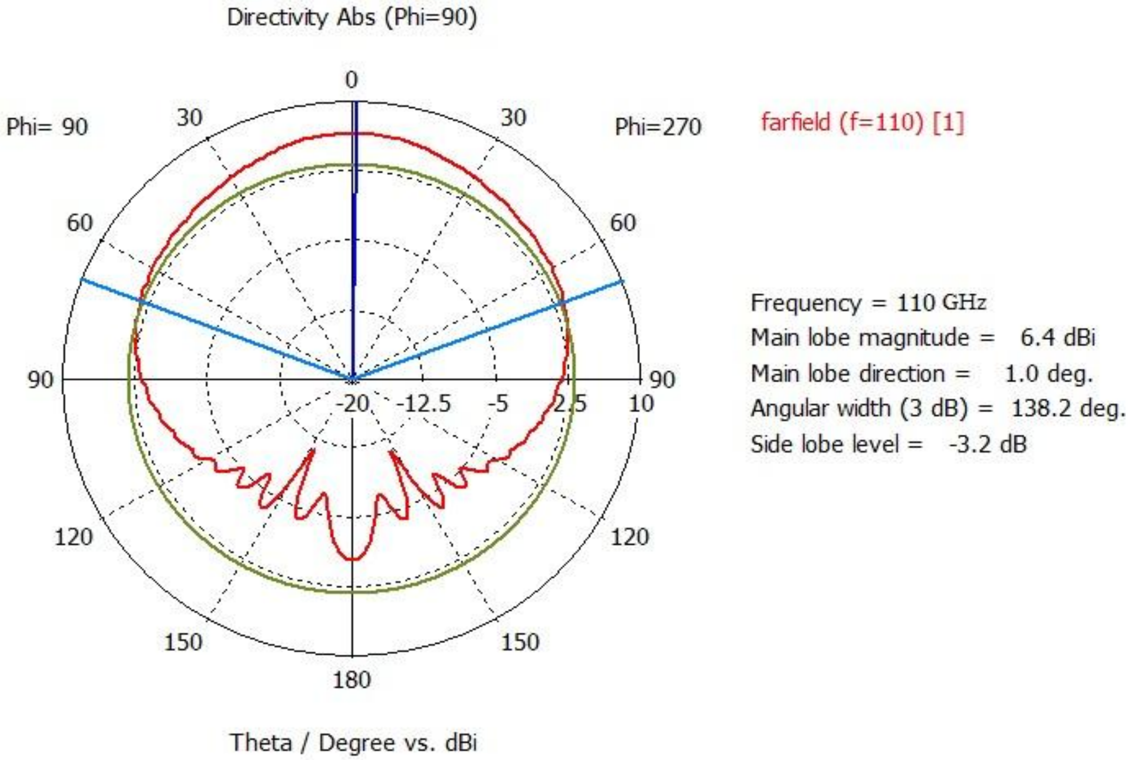

Fig. 2-14. E-Plane radiation pattern of a completely tapered WR-8 waveguide.

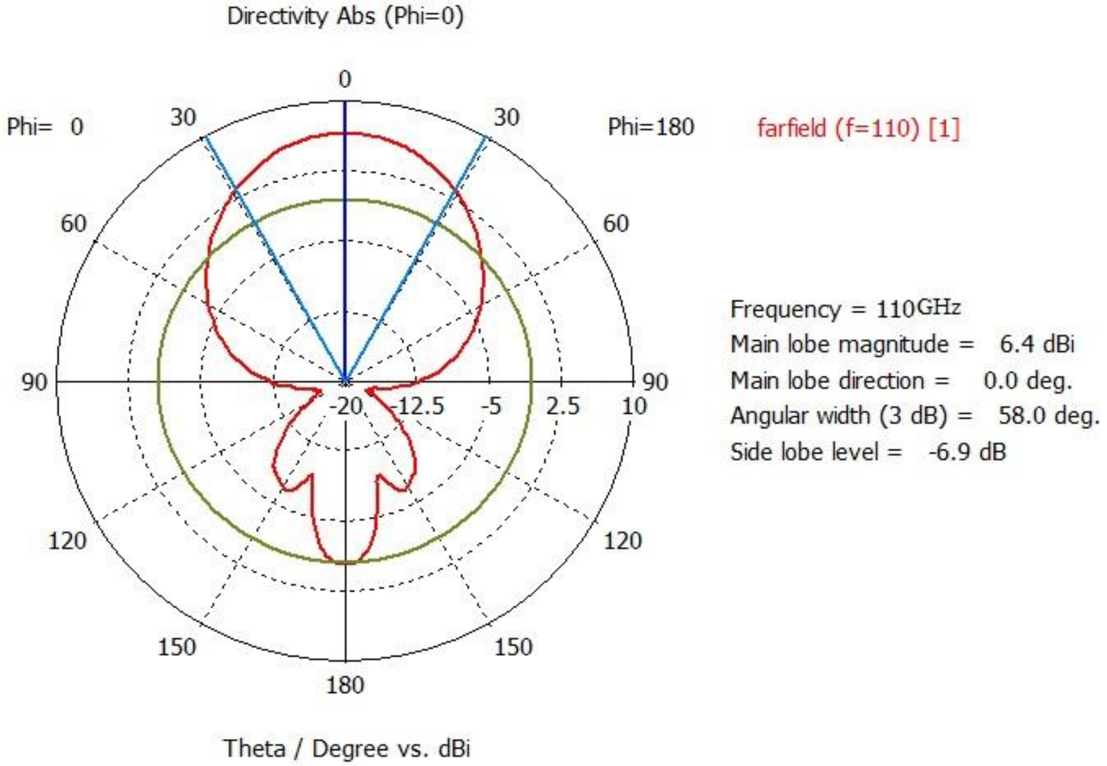

Fig. 2-15. H-Plane radiation pattern of a completely tapered WR-8 waveguide.

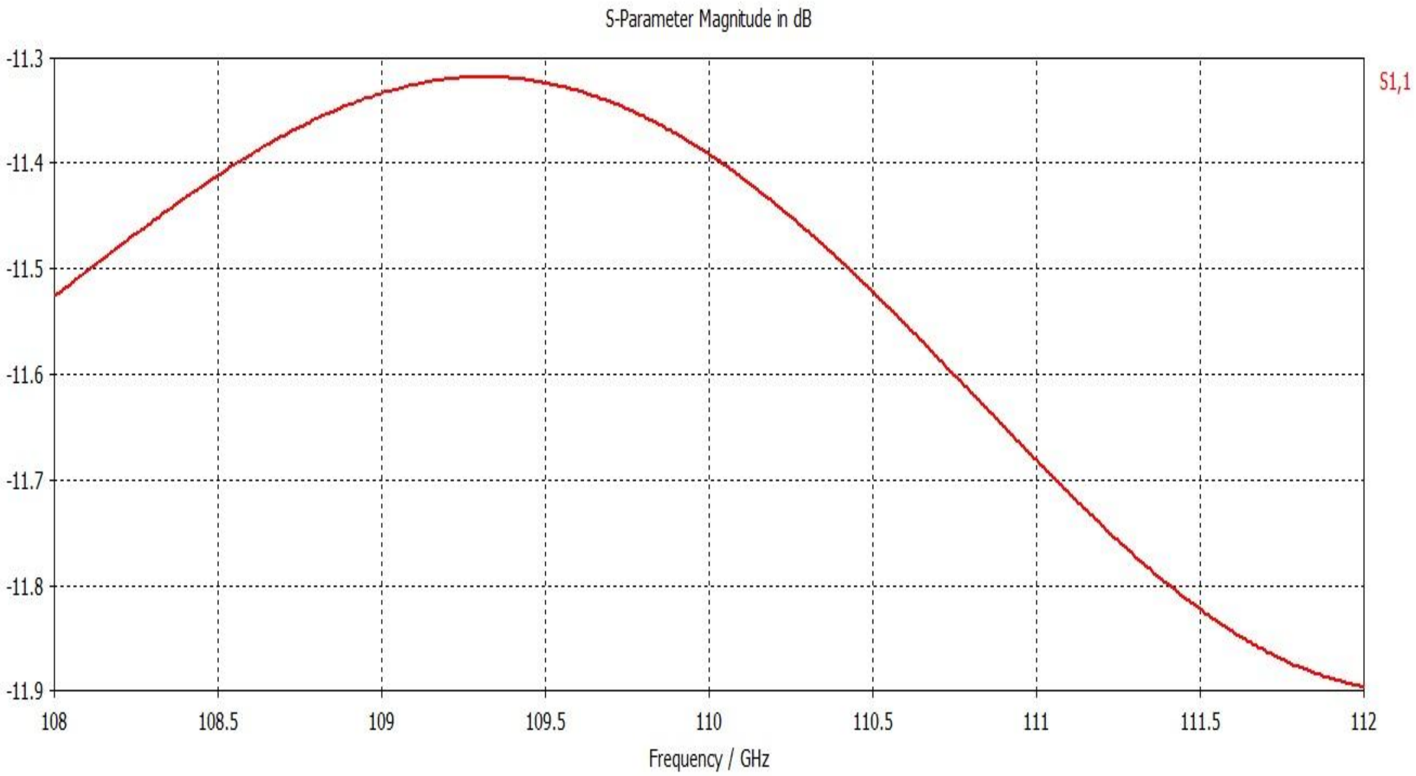

Fig. 2-16. Reflection Coefficient S_{11} (dB) of a completely tapered WR-8 waveguide.

In order to verify the simulation results, the WR-8 waveguide at 110 GHz is scaled down to corresponding lower frequency in the X-band using the similitude principle and the radiation patterns in E-plane and H–plane are compared in Fig. 2-17 and Fig. 2-18.

For WR-8 (F-band) waveguide: - a = 2.03 mm, b = 1.02 mm and f = 110 GHz

Outer dimensions: - a = 2.26 mm, b = 1.28 mm

For WR-90 (X-band) waveguide: - a = 22.86 mm, b = 10.16 mm

$$\text{Scaling factor} = \frac{22.86}{2.03} = 11.261$$

According to similitude principle, as the dimension is scaled by a factor of 11.261 then the frequency should also be scaled by a factor of 1/11.261. Hence it becomes,

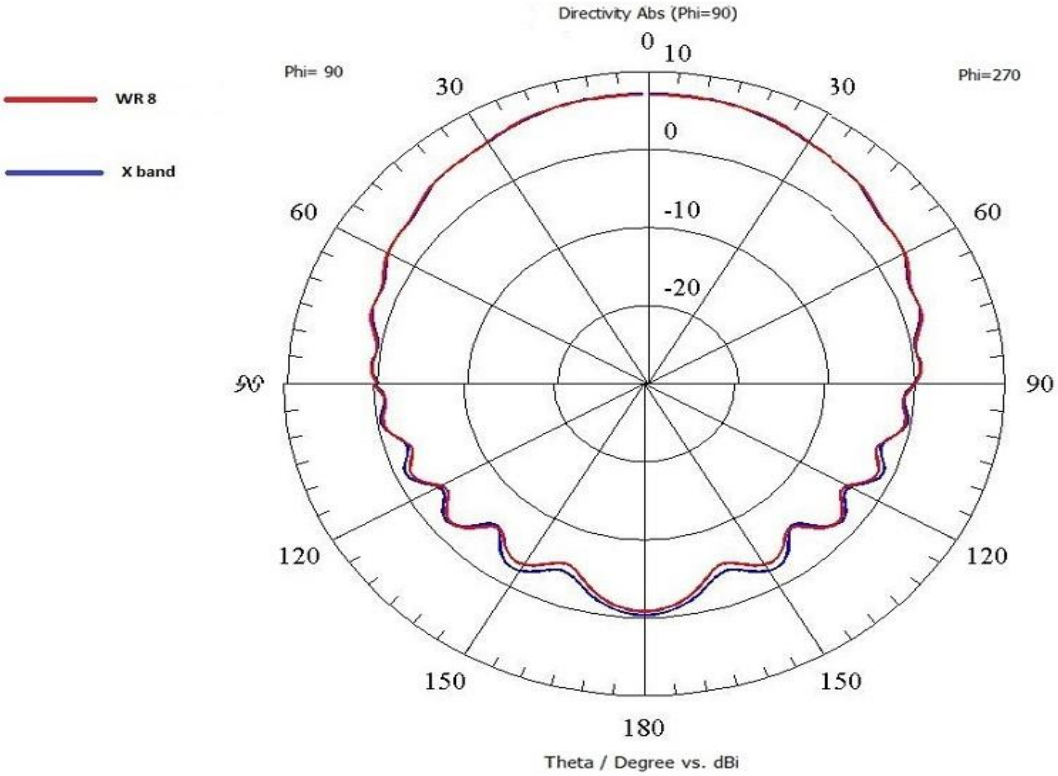

Fig. 2-17. E-Plane radiation patterns.

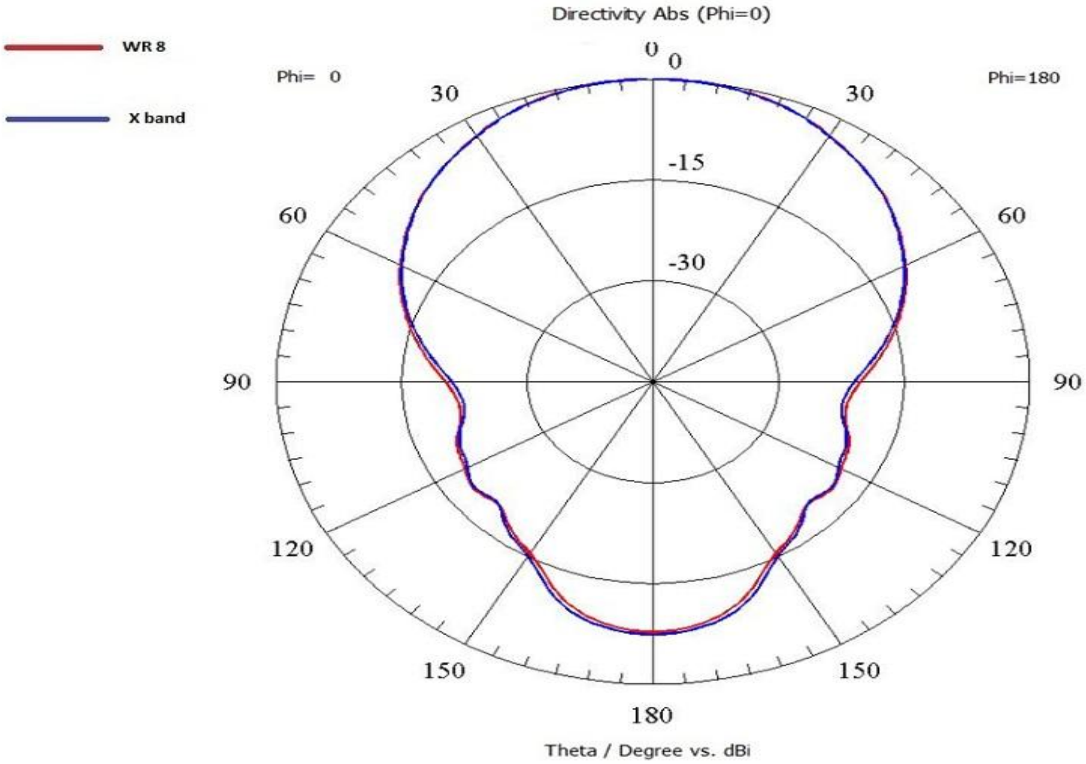

Fig. 2-18. H-Plane radiation patterns.

$$\text{Scaled frequency} = \frac{110GHz}{11.261} = 9.768\text{ GHz}$$

A very good agreement between both the radiation patterns of Scaled WR-8 and X-band waveguide is observed. These simulated scaled X-band results are also compared with the data published in [1] and is tabulated in Table 2-1.

Parameter	**Yaghjian's Paper**	**Simulated**
E- plane HPBW	114°	109.9°
H-plane HPBW	62°	64°
E-plane -6 dB Beam width	172	171°
H-plane -6 dB Beam width	90°	90.6°
Magnitude of reflection coefficient (S_{11})	-10.46 dB	-12.04 dB

Table: 2-1. HPBW and S11 from Yaghjian's paper and for X band waveguide at f = 9.32 GHz.

It can be concluded that there is a reasonable agreement between the two sets of values.

CHAPTER 3

A TE$_{0n}$ VLASOV LAUNCHER – A CIRCULAR WAVEGUIDE WITH A BAFFLE

In circular waveguides for TE$_{0n}$ modes, as the frequency increases for a fixed guide radius the metal losses get smaller. Hence, these modes are of interest for high frequency, high power applications. In this study, one such mode, the TE$_{02}$, is analyzed at 60 GHz. The problem of studying a circular waveguide with baffle is broken down into two parts. The first being analyzing the circular waveguide alone as shown in Fig. 3-1 and the second is to analyze a circular waveguide with the baffle as shown in Fig. 3-4.

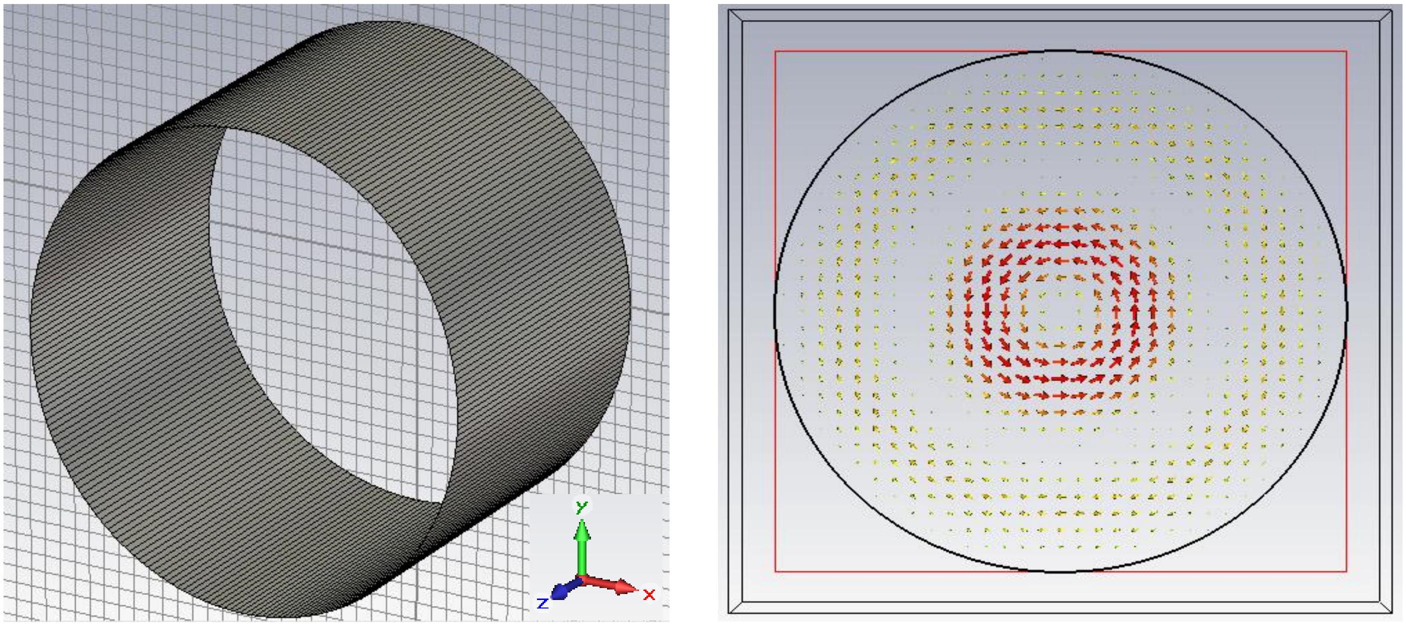

Fig. 3-1. A circular waveguide with a diameter $2a$ = 1.094” and excited TE$_{02}$ mode distribution at the port of the circular waveguide (right).

The cut-off frequency f_c for the TE$_{02}$ mode is calculated by knowing the zero of the derivative of the Bessel function for TE$_{02}$, $\chi'_{02} = 7.015587$

Therefore, for the given radius a$= 1.094'' * 2.54/2 = 1.38938$ cm,

$$\beta_c = \chi'_{02}/a = 5.049437 \text{ rad/cm}$$

$$f_c = \beta_c * c/2\pi = 24.109287 \text{ GHz} \quad (\because c = 3x10^{10} \text{ cm/s})$$

The simulation of the given geometry gives a cut-off frequency f_c for the TE_{02} mode as,

$$f_c = 24.1133 \text{ GHz}$$

which is reasonably close.

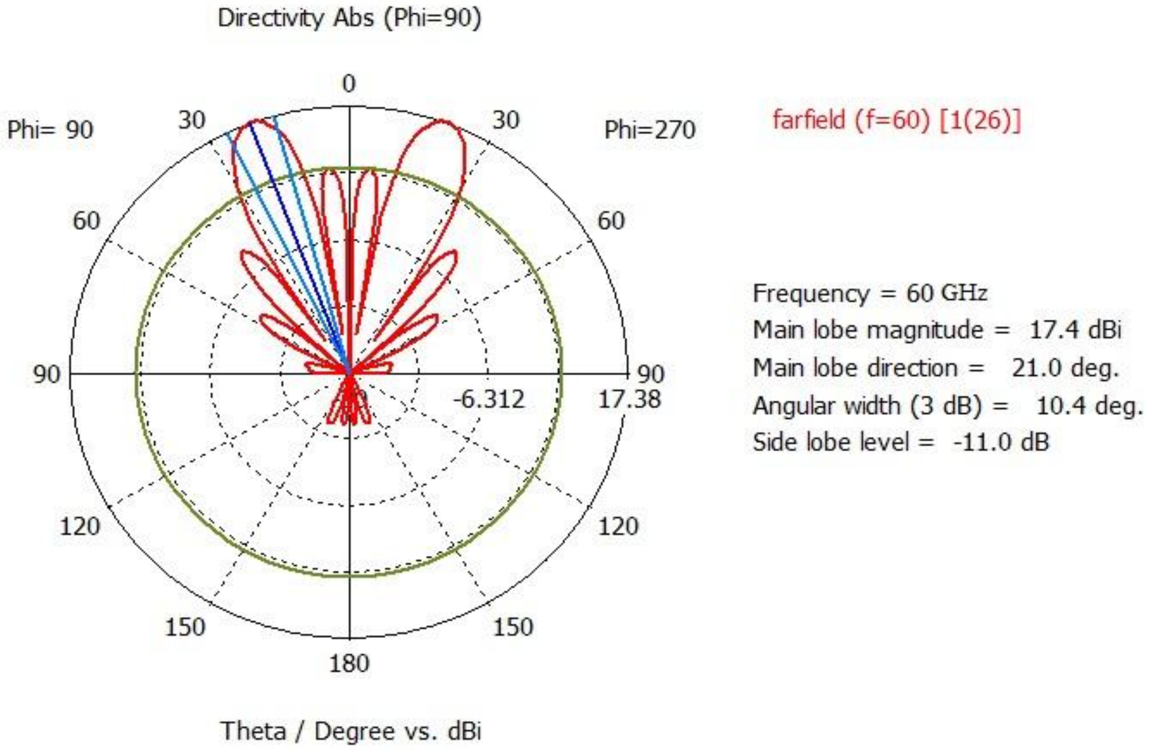

Fig. 3-2. Radiation pattern at φ = 90° of a TE_{02} mode in a circular waveguide with a diameter = 1.094".

The radiation pattern of a circular waveguide at φ = 90° is shown in Fig. 3-2. The green circle in all the radiation patterns represents the side lobe level which is the side lobe of the minor lobes with maximum intensity out of all minor lobes located outside the angular width of the main lobe. It is also known that at 60 GHz for $a = 1.094"$, there are five TE_{0n} modes (where n = 1 to 5) which can propagate. This corresponds to the five lobes in each forward quadrant of Fig. 3-2.

For the radiation patterns of TE_{0n} modes, if we consider only the terms which are function of θ, it is found [3] that the phi component of electric field E_φ is,

$$E_\varphi \propto \frac{ka\omega\mu\,(\frac{\beta mn}{k}+\cos\theta\,)\,J'_0(ka\ \sin\theta)}{\left[1-\left(\frac{ka\sin\theta}{\chi'_{0n}}\right)^2\right]} \qquad (\because m = 0\,)$$

Hence, for the given case of the TE_{02} mode, the peak in the radiation pattern occurs close to the second null of the derivative of the 0th order Bessel function which is verified in Fig. 3-3. It can also be seen from the same figure that remaining nulls of the 0th order Bessel function match reasonably well with nulls in the radiation pattern.

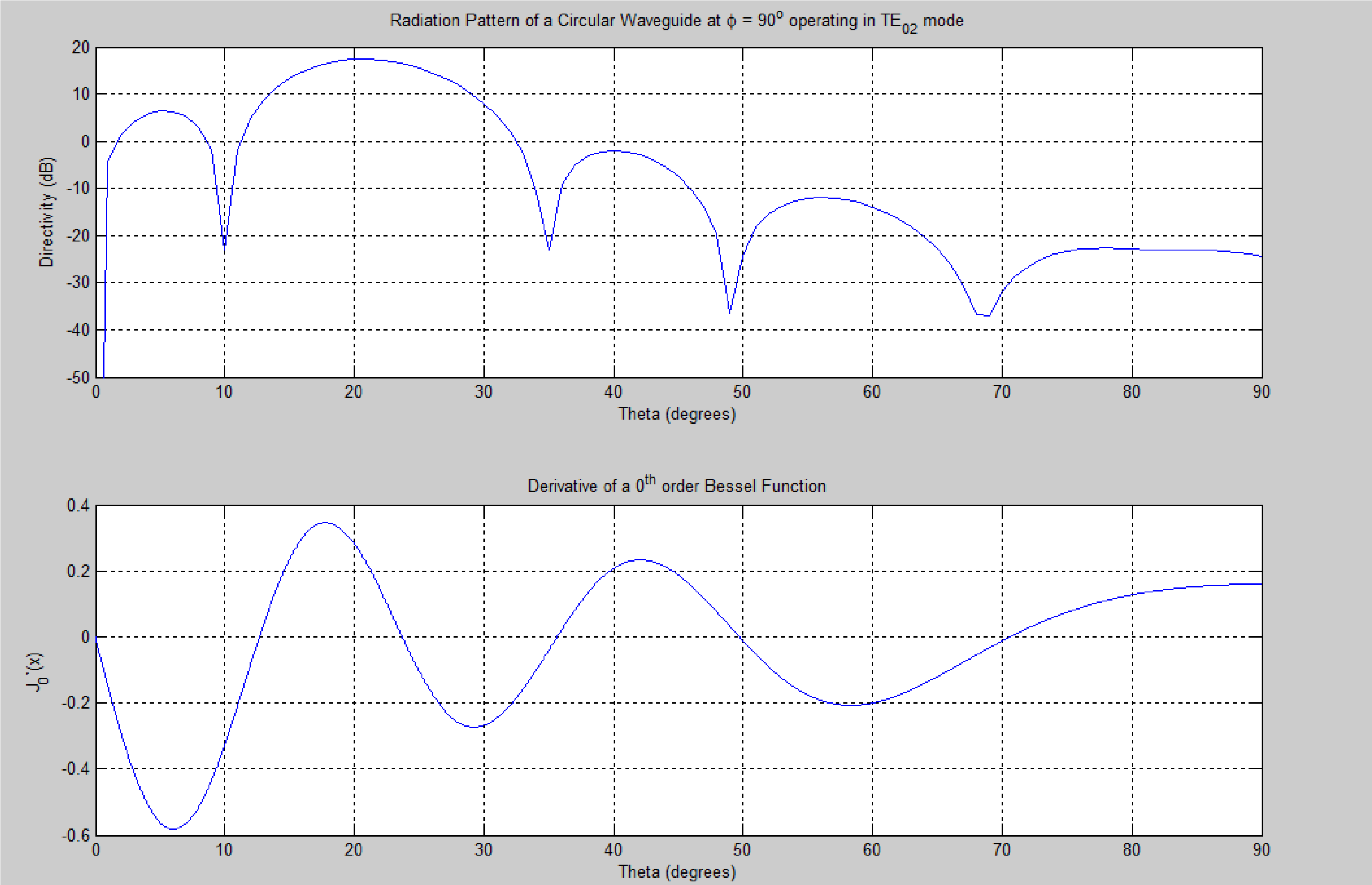

Fig. 3-3. Comparison of the nulls of a radiation pattern of a circular waveguide operating in TE_{02} mode as calculated with CST with the derivative of a 0th order Bessel function.

According to Geometrical Optics (GO) for a given mode, all rays inside the waveguide pass through a definitive area called Brillouin zone. It is periodic and when the waveguide is unfolded we get the Brillouin zone diagram for a given mode.

For a circular waveguide of radius $R_{W,}$ the field of a rotating wave with azimuthal index m and radial index n or of a TE$_{0n}$ mode has the form,

$$F = \frac{g_{mn}}{k} J_m(g_{mn} r) \exp\,(im\emptyset\ + ih_{mn}z + i\omega t\ )$$

where, F is the longitudinal component of the electric field E_z (for the TM modes) or magnetic field H_z (for TE modes) fields, $g_{mn} = v_{mn}/R_W$ and h_{mn} are transverse and longitudinal wavenumbers, respectively. v_{mn} is the root of the equation $J_m(v_{mn}) = 0$ or $J_m^{'}(v_{mn}) = 0$ for TM and TE modes, respectively. J_m is a Bessel function of the first kind of order m, $(r, \emptyset, z)$ is the cylindrical coordinate system, the z axis is directed along the waveguide axis, and k is the wavenumber [2].

At f =60 GHz, $\lambda = 0.5$ cm

hence, $k = \frac{2\pi}{\lambda} = 12.56637$ rad/cm.

Between two reflections from the waveguide walls, each ray, travels a distance along the waveguide axis which is called as bounce length L_{B} ,

$$L_B = \frac{2R_W}{\tan\theta} \sqrt{1 - \left(\frac{m}{v_{mn}}\right)^2} \tag{3-1}$$

where,

$$\theta_B = \arcsin\,(g_{mn}/k) \tag{3-2}$$

is the Brillouin angle.

For the TE$_{mn}$ modes ,

$$J_m'(v_{mn}) =\ 0$$

Therefore, in our case for the TE$_{0n}$ mode where m = 0 and n = 2 it becomes,

$$J_0'(v_{02}) =\ 0$$

which is satisfied when $v_{02} = 7.0156$

$$g_{mn} = v_{mn}/R_W$$

In our case, $R_W = 1.094''/2 = 1.38938$ cm ,

$$g_{02} = 5.04945 \text{ rad/cm}$$

From the given geometry, Eq. (3-2) and Eq. (3-1) gives,

$$\theta_B = 23.692°$$

and

$$L_B = 6.33255 \text{ cm}$$

The simulation of this circular waveguide with baffle is carried out using CST Microwave Studio. The structure simulated in CST is shown in Fig. 3-4.

It can be seen from Fig. 3-5 that, the angle of the main lobe occurs at $\theta_B = 19.5°$ for a bounce length of $L_B = 6.33255$ cm. The radiation pattern of the circular waveguide with baffle at $\varphi = 90°$ using Surf and CST software are shown in Fig. 3-6 and Fig. 3-7 respectively. The shape of the graphs matches reasonably well.

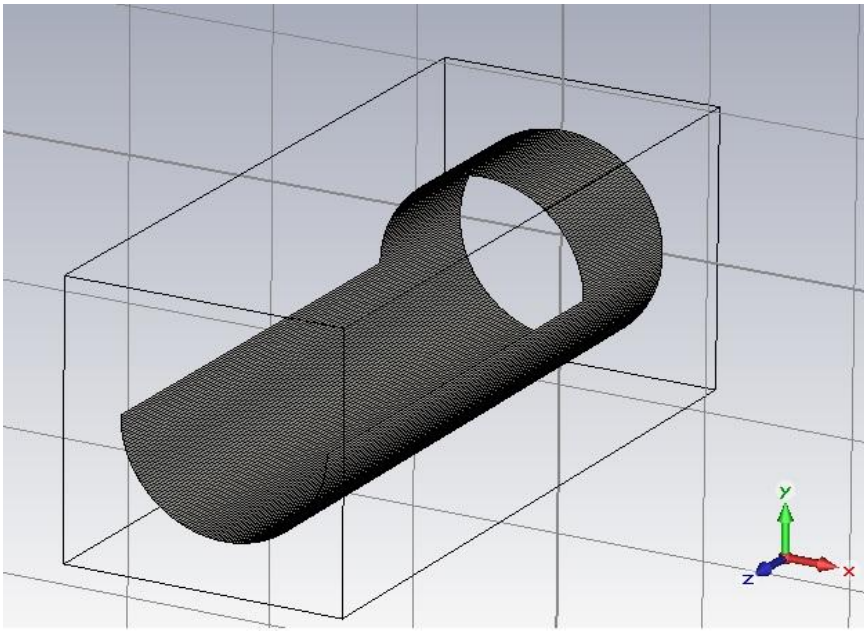

Fig. 3-4. A circular waveguide with a diameter = 1.094” with a baffle of length $L_{B\,=}$ 6.33255 cm.

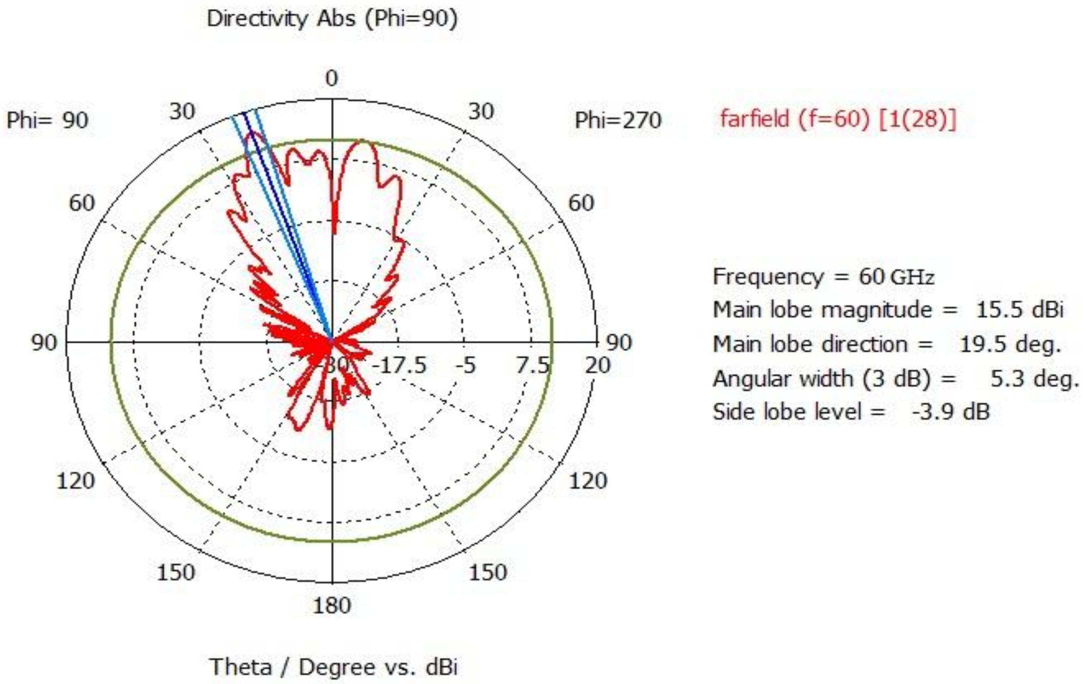

Fig. 3-5. Radiation pattern of the circular waveguide with baffle at φ = 90°.

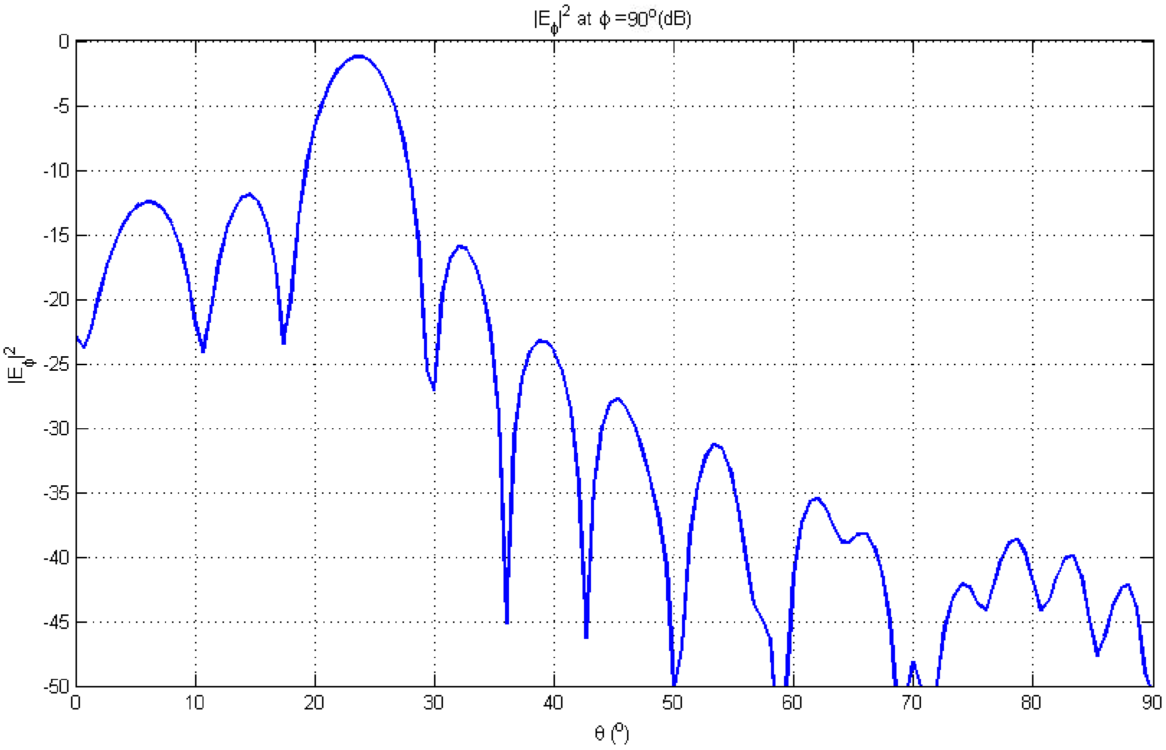

Fig. 3-6. Surf simulation of the launcher with a baffle length L_B = 6.33255 cm at φ= 90°.

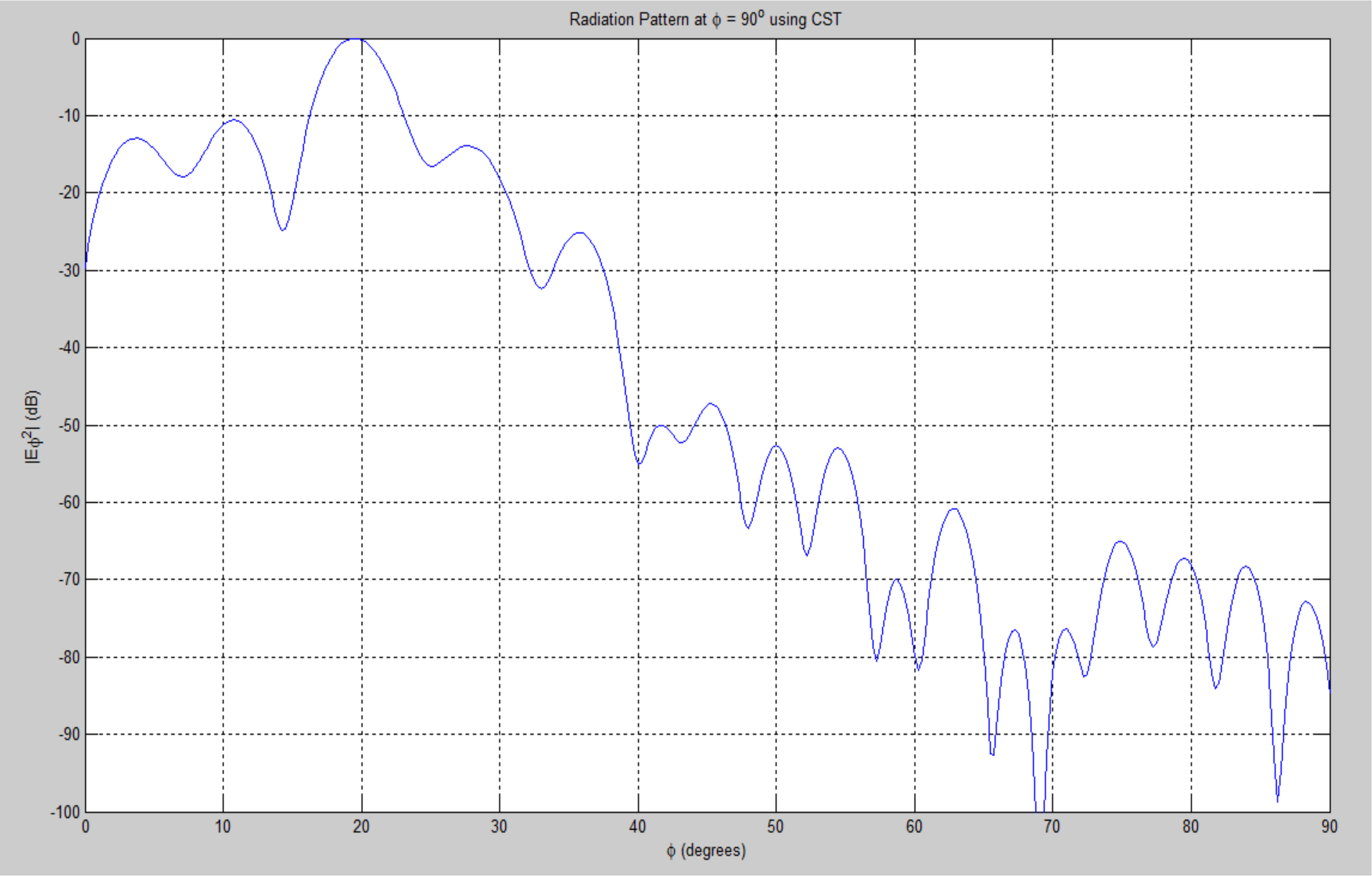

Fig. 3-7. Radiation pattern of the launcher operating in TE_{02} mode using CST at φ= 90°.

CHAPTER 4

PART A

EQUATIONS AND GRAPHS FOR THE EXPANSION OF A GAUSSIAN BEAM

Gaussian beams are like plane waves in many aspects. However instead of being a uniform distribution, their intensities are concentrated near the axis of propagation and the phase fronts are slightly curved. The beam which is being circulated inside the resonator is being generated by a Gaussian beam horn. The following figure shows that when the circular waveguide modes come to the end of the waveguide, they radiate an approximate Gaussian mode in space [4]. This mode will spread by diffraction in space as shown in Fig. 4-1.

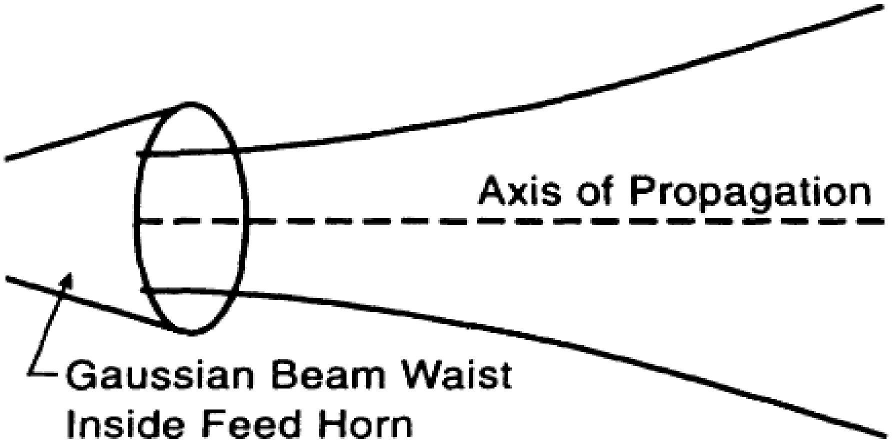

Fig. 4-1. Gaussian beam produced by a feed horn.

A rectangular E field component of the beam satisfies the scalar Helmholtz equation,

$$\nabla^2 E + k^2 E = 0 \tag{4-1}$$

where, $k = 2\pi/\lambda$ is the propagation constant in the medium.

Hence, the main propagation variation in the homogeneous region still has a factor of e^{-jkz}. In addition to the other variations with z, the field can be mathematically expressed as,

$$E(\rho, \phi, z) = \psi(\rho, \phi, z)\, e^{-jkz} \tag{4-2}$$

where, ψ is a slowly varying complex function which illustrates the difference between a plane wave and a diverging Gaussian beam. To derive ψ, we solve for the solution to the paraxial equation in cylindrical coordinates,

$$\frac{\partial}{\rho \partial \rho}\left(\rho \frac{\partial \psi}{\partial \rho}\right) + \frac{1}{\rho^2}\frac{\partial^2 \psi}{\partial \phi^2} - 2jk\frac{\partial \psi}{\partial z} = 0 \tag{4-3}$$

For the fundamental mode, there is no ϕ variation. Then the equation reduces to,

$$\frac{\partial}{\rho \partial \rho}\left(\rho \frac{\partial \psi}{\partial \rho}\right) - 2jk\frac{\partial \psi}{\partial z} = 0 \tag{4-4}$$

The solution to this paraxial equation can be obtained in the form,

$$\psi = \exp\left[-j\left(P + \frac{k}{2Q}\rho^2\right)\right] \tag{4-5}$$

where, P(z) represents a complex phase shift with the propagation of the wave and Q(z) is a complex beam parameter which illustrates how the amplitude of the Gaussian beam varies with distance ρ from the z axis.

$$\frac{1}{Q(z)} = \frac{1}{R(z)} - \frac{2j}{kw^2(z)} \tag{4-6}$$

where, R(z) is the radius of curvature of the spherical wavefronts, as shown in Fig. 4-2, and w(z) is a measure of the Gaussian beam radius at position z. Mathematically, w(z) is the radius ρ at which the beam amplitude is $\frac{1}{e}$ of it's value at ρ = 0 for that value of z. Therefore, the real part of $\frac{1}{Q(z)}$ gives the phase related to the curvature of the wavefront and the imaginary part gives the Gaussian amplitude variation with radius. After some algebraic manipulation, the fundamental mode E field of the Gaussian beam can be expressed as,

$$E(\rho, z) = E_0 \frac{w_0}{w(z)} \, exp\left[-\frac{\rho^2}{w^2(z)}\right] \, \phi(\rho, z) * e^{-jkz} \qquad (4\text{-}7)$$

where,

$$\phi(\rho, z) = \exp[-j(\frac{k\rho^2}{2R(z)} - T(z)] \qquad (4\text{-}8)$$

$$w(z) = w_0 \left(1 + \frac{z^2}{z_R^2}\right)^{\frac{1}{2}} \qquad (4\text{-}9)$$

$$R(z) = z + \frac{z_R^2}{z} \qquad (4\text{-}10)$$

$$T(z) = \arctan(\frac{z}{z_R}) \qquad (4\text{-}11)$$

$$z_R = \frac{kw_0^2}{2} \qquad (4\text{-}12)$$

E_o is an amplitude constant and ρ is the cylindrical coordinate radius. $\phi(\rho, z)$ is the phase function of the wave to give the phase difference between the Gaussian beam and the ideal plane wave, z_R is called the Rayleigh distance and w_0 is the beam radius at the beam waist where the phase front is planar. The amplitude factor $\frac{w_0}{w(z)}$ gives the expected intensity decrease on the z axis due to expansion of the beam [5]. Fig. 4-2 shows the variation of the beam radius $w(z)$ varies as a function of z. It is important to note that for $z \gg z_R$ the beam radius approaches a linear asymptote which is also verified using a MATLAB code.

Fig. 4-3 shows a series of the amplitude plots of a Gaussian beam, which propagates in the z-direction. Note that the beam spreads as it propagates and it’s amplitude decreases with z while maintaining a Gaussian form for each position of z. In a lossless medium, the beam will carry constant power.

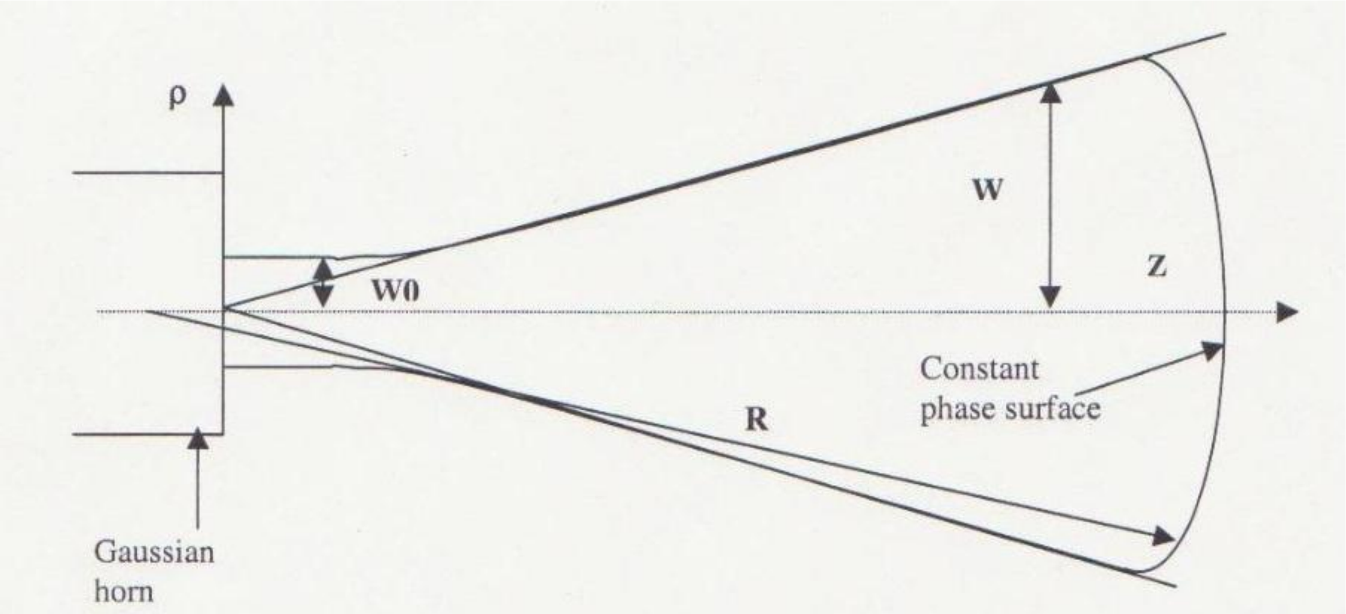

Fig. 4-2. Gaussian beam after leaving the Gaussian horn, will spread by diffraction effects.

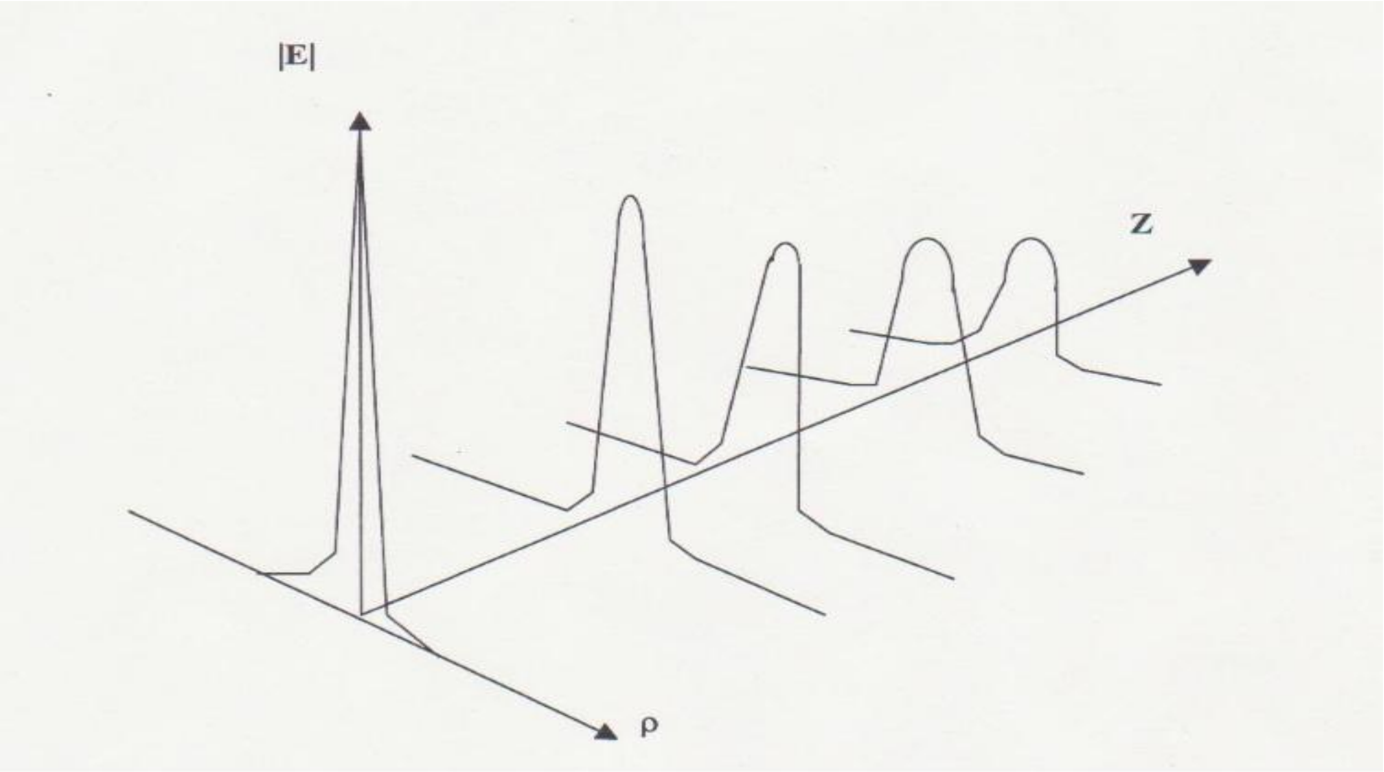

Fig. 4-3. Gaussian beam amplitude as a function of ρ and z.

The mirror with a coupling iris is designed so that the -30 dB power contour is on its surface to make sure most of the power is being captured. The dimensions of the mirror are finalized taking into account an oblique incidence of the Gaussian beam. Amplitude of the E-field is represented by Eq. (4-13). The distribution of power of the Gaussian beam as a function of ρ, z is plotted for two different cases using MATLAB. In both the cases, the result is plotted for -8.68 dB (1/e^2), -20 dB and -30 dB power contours. The waist of the Gaussian beam is $w_0 = 0.57 * a = 6.75$ mm, where $2a = 23.68$ mm is the diameter of the Gaussian beam horn antenna.

Case 1:- In this case, the power contours are plotted considering the amplitude of the E field to be,

$$E(\rho, z) = E_0 \frac{w_0}{w(z)} \, exp\left[-\frac{\rho^2}{w^2(z)}\right] \tag{4-13}$$

and the result is shown in Fig.4-4.

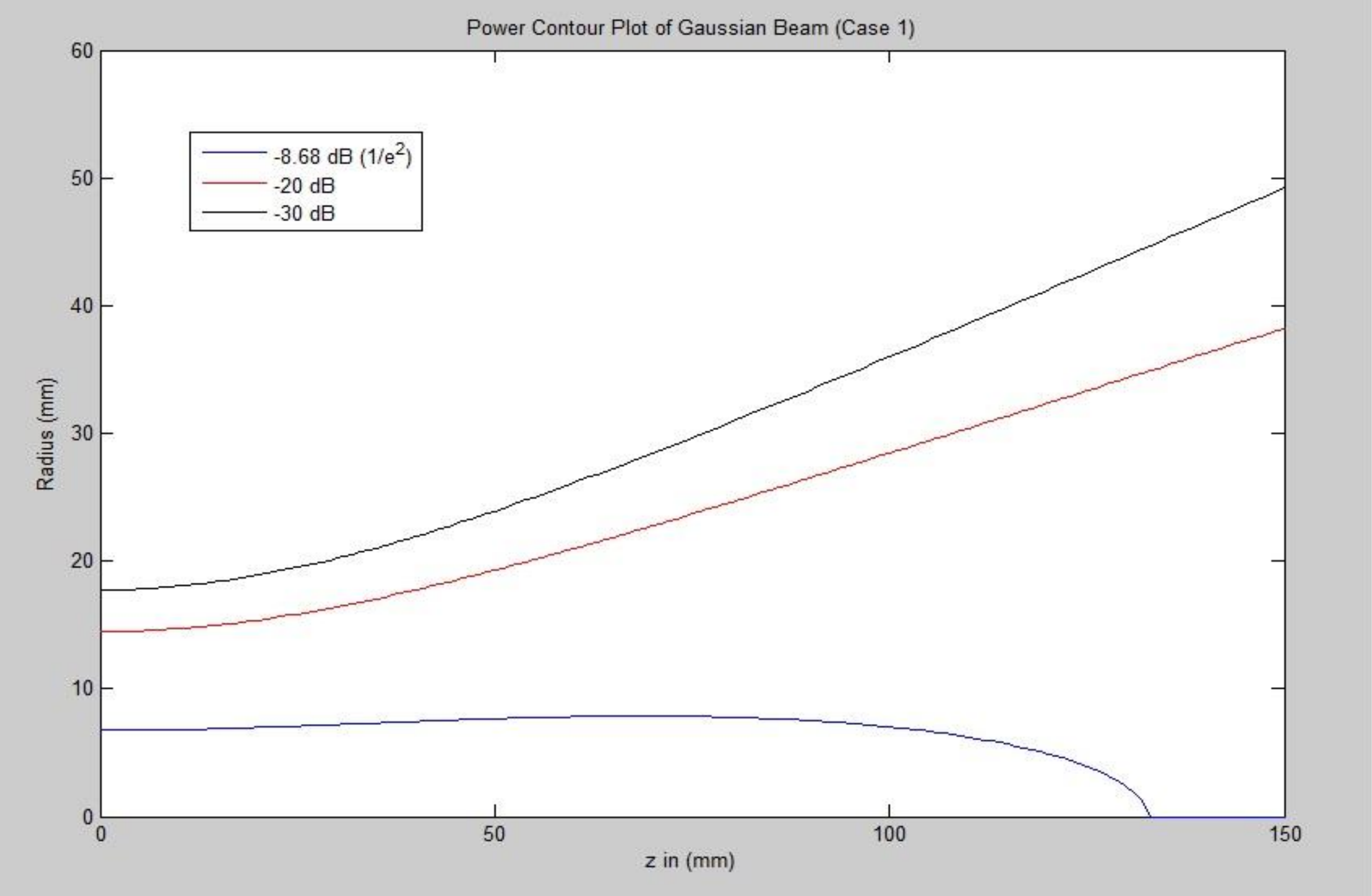

Fig. 4-4. Power contour plot of a Gaussian Beam (Case 1) for a waist $w_0 = 0.675$ mm.

Case 2:- In this case, the power contours are plotted considering the amplitude of E relative to the peak value at that value of z,

$$E(\rho, z)/E_0 \quad = exp\left[-\frac{\rho^2}{w^2(z)}\right] \tag{4-14}$$

and the result is shown in Fig.4-5.

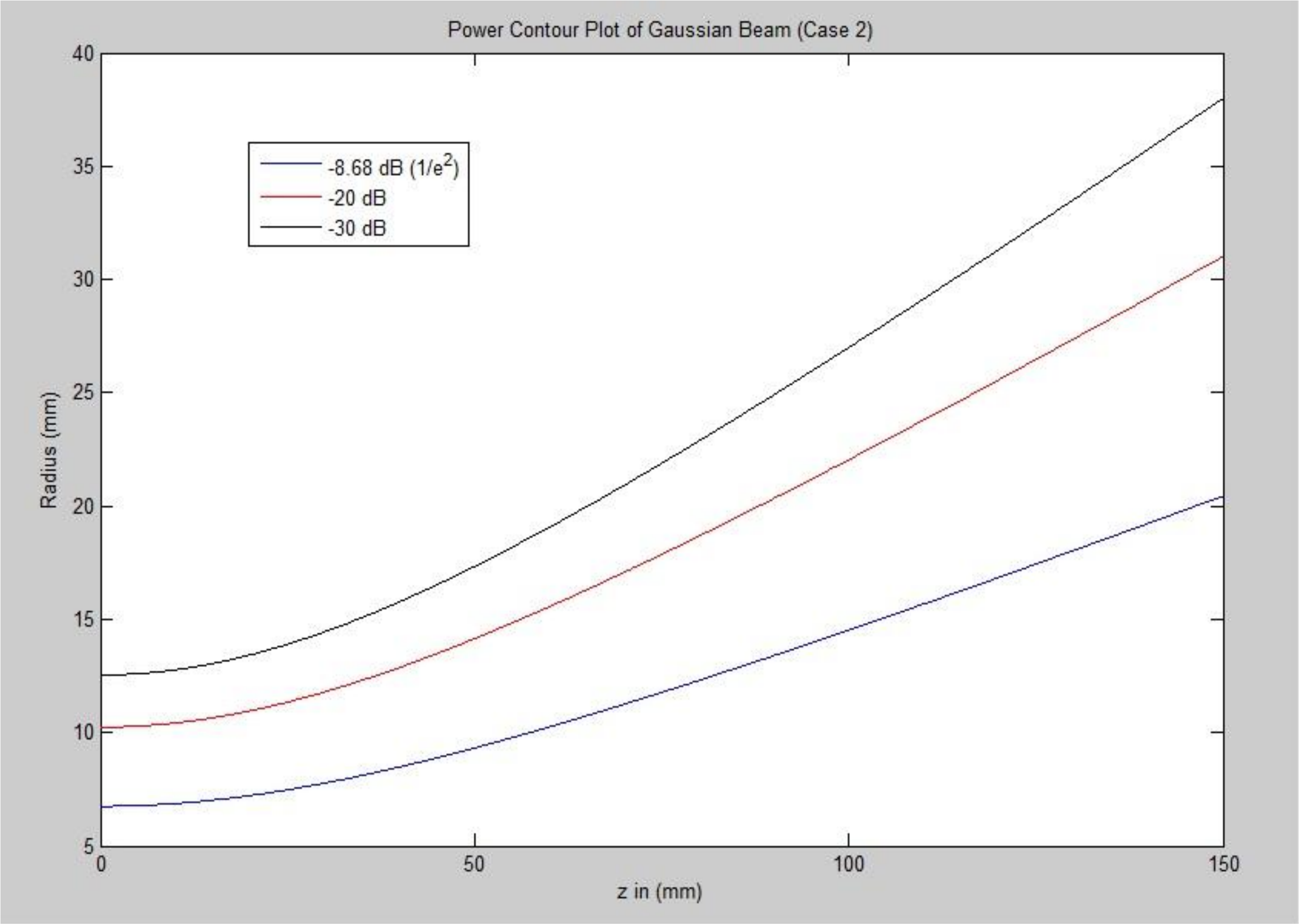

Fig. 4-5. Power contour plot of a Gaussian Beam (Case 2) for a waist $w_0 = 0.675$ mm.

The dimensions of the mirror which has the coupling iris are chosen based on the plots shown above. Assuming an angle of incidence of 45°, the dimensions of the mirror are tabulated in the Table. 4-1 based on the positioning of the mirror for different values of z.

Distance along z (cm)	Length of the mirror (cm)	Width of the mirror (cm)
15	11.6	7.75
20	14.5	10
25	18.4	12.25

Table: 4-1. Dimensions of the mirror based on positioning in z.

In order to study a less divergent beam, plots similar to Fig. 4-4 and Fig. 4-5 are shown in Fig. 4-6 and Fig. 4-7 for a waist $w_0 = 2$ cm. One of the ways to get this waist is by putting the Gaussian beam

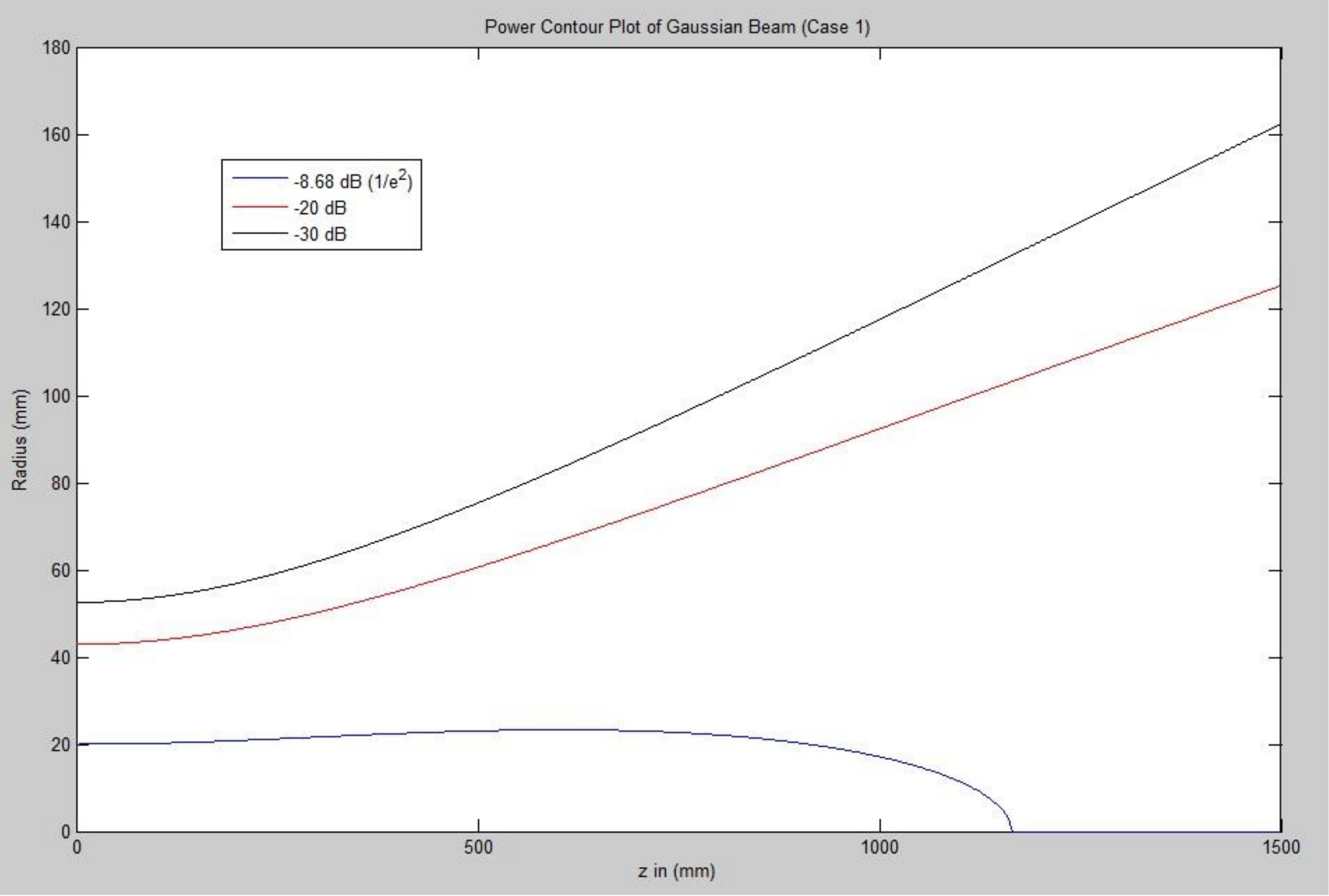

Fig. 4-6. Power contour plot of a Gaussian Beam (Case 1) for a waist $w_0 = 2$ cm.

generated by the horn antenna onto the mirror which helps to get the required waist.

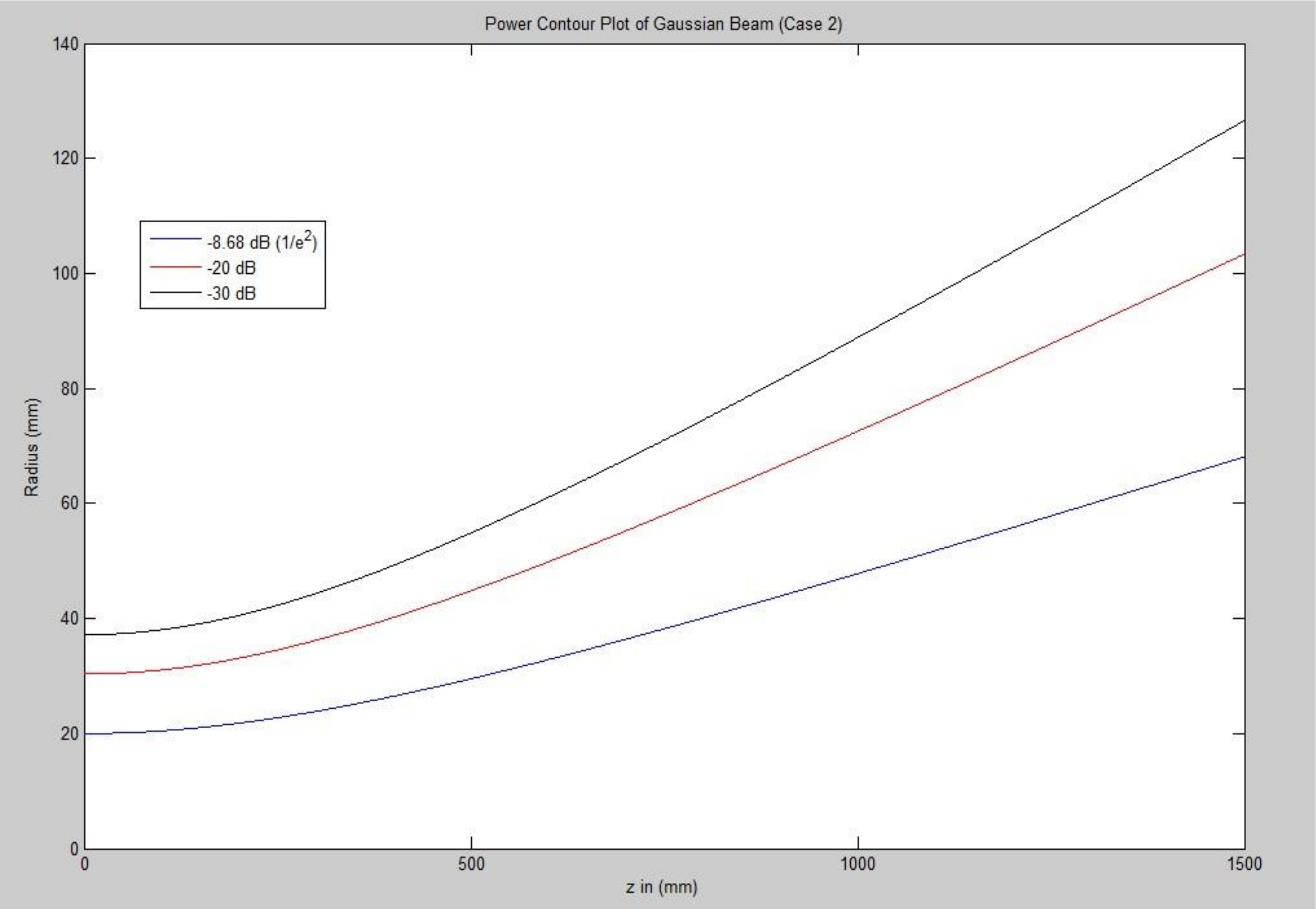

Fig. 4-7. Power contour plot of a Gaussian Beam (Case 2) for a waist $w_0 = 2$ cm.

PART B

COUPLING HOLE FOR A TRAVELLING WAVE RESONATOR AT 110 GHz

The testing of high power-handling capacity of microwave devices [6], can be done using the proposed travelling wave resonator shown in Fig. 4-8. The input signal is a Gaussian beam coming out of a Gaussian beam circular horn. When the signal hits the diffraction grating, the diffracted beam circulates inside the resonator if the path length of the signal inside the resonator is chosen correctly. The angle of the diffracted beam is calculated using Eq. (4-15).

$$\theta_n = \arcsin\left(\sin\theta_i - \frac{n\lambda}{P}\right) \tag{4-15}$$

where n, P, θ_i represent order of diffraction, the period of grating and the angle of incidence respectively.

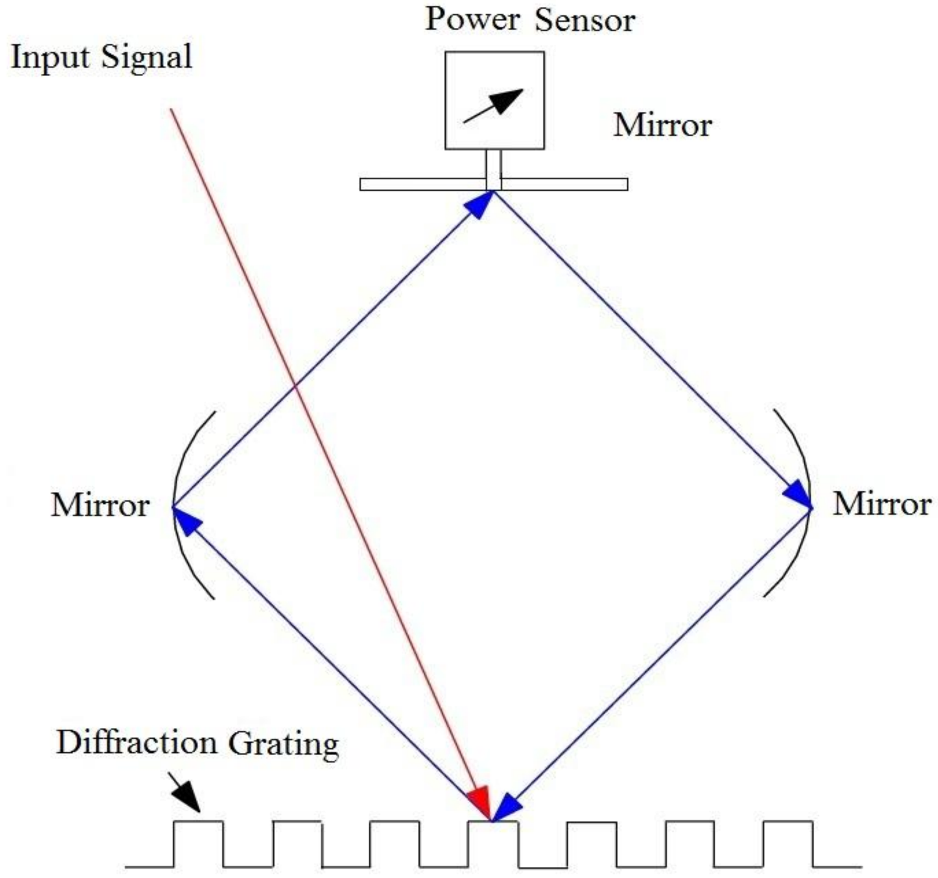

Fig. 4-8. Experimental set up of a travelling wave resonator.

The amount of power inside the resonator can be measured with the help of a small hole in one of the mirrors which is also known as coupling hole. The diameter of coupling hole is chosen such that the fields in the resonator are minimally perturbed [7], [9]. The increase in the signal is expected to be of the order of 4-5 times the original.

The beam circulating inside the resonator is desired to be circular in cross section. We propose to use an elliptical Gaussian beam as the input signal so that the diffracted beam is a circular Gaussian beam and then adjust the orientation and/or position of the three mirrors precisely such that the power in the resonator adds up.

COUPLING HOLE

The detailed diagram of the coupling hole and the attached assembly is shown in Fig. 4-9. The coupling hole is connected to a power sensor with the help of a circular to rectangular waveguide transition. The radius of the hole, to be equal to a = 0.9525 mm, is chosen so that only one mode i.e the dominant TE_{11} mode propagates in the circular waveguide.

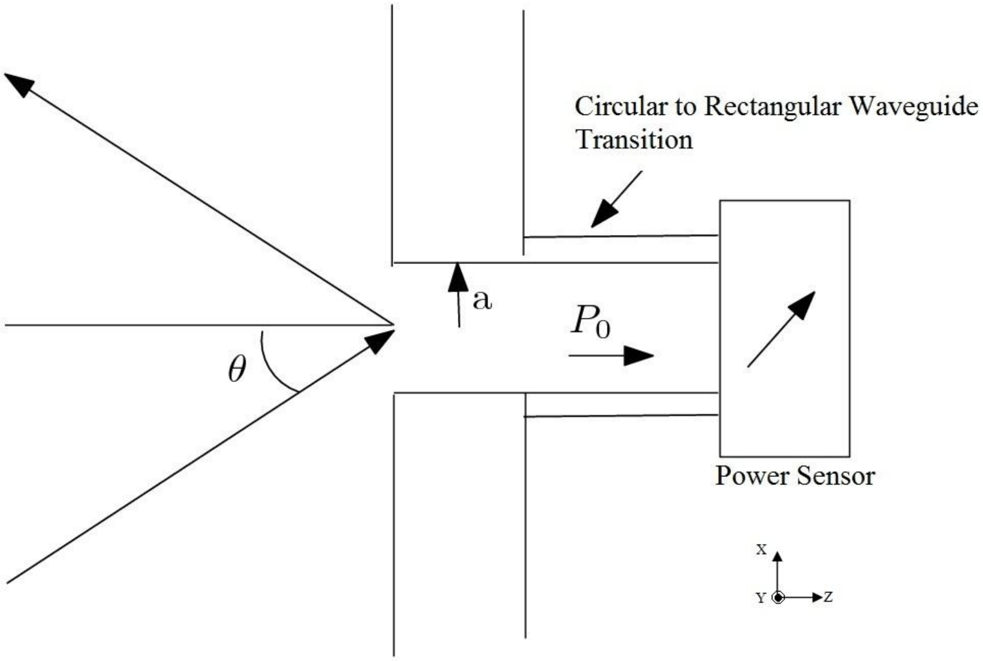

Fig. 4-9. Coupling hole and the remaining assembly.

In a circular waveguide the first two modes with lowest cut-off frequencies are TE_{11} and TM_{01}. The electric field expressions of these modes are given in Equations (4-16)-(4-20). Corresponding magnetic fields can be calculated by knowing the intrinsic impedance η of the medium filling the waveguide which is free space in this case. The electric and magnetic field configurations inside the waveguide are shown in Fig. 4-10 [8].

TE_{11} *(equations* 4-16, 4-17*)* and TM_{01} *(equations* 4-18, 4-19*)*

$$\boldsymbol{E_\rho} = -A\, J_1(\beta_\rho \rho)[-C\sin(\varphi) + D\cos(\varphi)]\, e^{-j\beta_z z} \tag{4-16}$$

$$\boldsymbol{E_\varphi} = -A\, J_1'(\beta_\rho \rho)[C\cos(\varphi) + D\sin(\varphi)]\, e^{-j\beta_z z} \tag{4-17}$$

$$\boldsymbol{E_\rho} = -\frac{B\beta_\rho\beta_z}{\omega\varepsilon\mu}\, J_0'(\beta_\rho \rho)\, e^{-j\beta_z z} \tag{4-18}$$

$$\boldsymbol{E_z} = -\frac{jB\beta_\rho^2}{\omega\mu\varepsilon}\, J_0(\beta_\rho \rho)\, e^{-j\beta_z z} \tag{4-19}$$

and

$$' = \frac{\partial}{\partial(\beta_\rho \rho)} \tag{4-20}$$

where ω,β,μ,ε represent angular frequency, propagation constant, permeability and permittivity of the medium respectively. The subscript denotes the corresponding entity in the given direction. *A, B, C* and *D* are constants.

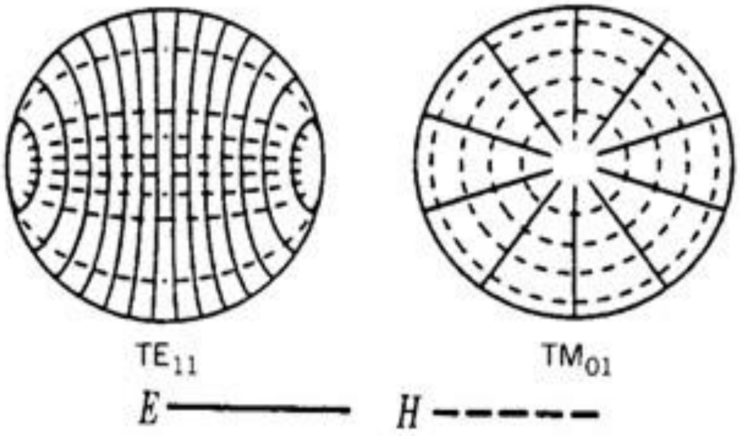

Fig. 4-10. Electric and magnetic field configuration of TE_{11} and TM_{01} mode in a circular waveguide.

The cut-off frequency f_c associated with each mode is calculated by knowing the corresponding zero of the derivative of Bessel function or the zero of the Bessel function for the TE or TM modes respectively. For the above mentioned modes it is calculated as,

a) For TE_{11} mode :- $\chi'_{11} = 1.841184$

$$f_c = \frac{\chi'_{11}}{a} * \frac{c}{2\pi} \qquad (\because c = 3x10^8 \mathrm{m/s})$$

$$f_c = 92.294 \text{ GHz}$$

b) For next higher mode TM_{01}:- $\chi_{01} = 2.404826$

$$f_c = \frac{\chi_{01}}{a} * \frac{c}{2\pi} \qquad (\because c = 3x10^8 \mathrm{m/s})$$

$$f_c = 120.548 \text{ GHz}$$

At $f = 110$ GHz, it is verified that only the TE_{11} mode propagates for a = 0.9525 mm as it's $f_c < f$.

It can be seen from Fig. 4-10 that the TE_{11} mode has polarization degeneracy. Only a small fraction of input signal gets coupled to the iris; hence it is important to know how much power gets coupled to each mode [9]. The coupling between two waves can be calculated using Eq. (4-21).

$$C = \frac{\iint \boldsymbol{E_1}.\boldsymbol{E_2^*} ds}{\sqrt{\iint |\boldsymbol{E_1}|^2 ds \iint |\boldsymbol{E_2}|^2 ds}} \tag{4-21}$$

where $\boldsymbol{E_1}$, $\boldsymbol{E_2}$ are electric fields of the waves under consideration.

This equation becomes a bit complicated to solve analytically but can be solved fairly accurately numerically. For the given polarization of the wave in the resonator; we'll have to find out the amount of coupling between the input signal and the mode which exists inside the waveguide. It is also a function of angle of incidence of the incident wave. As we are dealing with a wide waist Gaussian beam, the field at the aperture of the coupling hole can be approximated by a plane wave. Therefore, while carrying out the calculation of coupling coefficient C using MATLAB, $\boldsymbol{E_1}$,$\boldsymbol{E_2}$ are assumed fields of the TE_{11} mode and a plane wave respectively.

There are going to be two scenarios based on the polarization of the incident Gaussian beam.

1. Perpendicular polarization.
2. Parallel polarization.

Case 1 will be discussed here but calculations for case 2 can also be carried out in a similar manner. The electric field expression for the plane wave is written using Fig. 4-9 as,

$$\boldsymbol{E_2} = E_0\, e^{-j\beta(x\sin\theta + z\cos\theta)}\ \hat{y}$$

where, θ is the angle of incidence of the Gaussian beam.

Converting the vector to cylindrical co-ordinates using $x = \rho\cos\varphi$, $y = \rho\sin\varphi$ and vector conversion, the above equation changes to,

$$\boldsymbol{E_2} = E_0 \sin\varphi\ e^{-j\beta(\rho\cos\varphi\sin\theta + z\cos\theta)}\ \hat{\rho} + E_0\cos\varphi\ e^{-j\beta(\rho\cos\varphi\sin\theta + z\cos\theta)}\ \hat{\varphi}$$

The TE$_{11}$ mode travelling inside the coupling hole can be represented as,

$$\boldsymbol{E_1} = A\frac{J_1(\beta_\rho\rho)}{\varepsilon\rho}\sin\varphi\ e^{-j\beta_z z}\ \hat{\rho} + A\, J_1'(\beta_\rho\rho)\,\frac{\beta_\rho}{\varepsilon}\cos\varphi\ e^{-j\beta_z z}\ \hat{\varphi}$$

By looking at Eq. (4-21) the constant terms in the equations presented above can be assumed to be equal to unity, then it becomes,

$$\boldsymbol{E_1} = \frac{J_1(\beta_\rho\rho)}{\rho}\sin\varphi\ e^{-j\beta_z z}\ \hat{\rho} + J_1'(\beta_\rho\rho)\,\beta_\rho\cos\varphi\ e^{-j\beta_z z}\ \hat{\varphi}$$

and

$$\boldsymbol{E_2} = \sin\varphi\ e^{-j\beta(\rho\cos\varphi\sin\theta + z\cos\theta)}\ \hat{\rho} + \cos\varphi\ e^{-j\beta(\rho\cos\varphi\sin\theta + z\cos\theta)}\ \hat{\varphi}$$

The limits of integration for variables ρ, φ are from 0 to a and 0 to 2π respectively. Calculating the numerator N of Eq. (4-21) first gives us,

$$N = \iint \left(\frac{J_1(\beta_\rho \rho)}{\rho} \sin^2 \varphi \; e^{-j\beta_z z} \; e^{j\beta(\rho \cos\varphi \sin\theta + z\cos\theta)} \right.$$

$$\left. + \; J_1'(\beta_\rho \rho)\, \beta_\rho \cos^2 \varphi \; e^{-j\beta_z z} \; e^{j\beta(\rho \cos\varphi \sin\theta + z\cos\theta)} \right) \rho d\rho \, d\varphi$$

$$= \iint e^{-j\beta_z z} e^{j\beta z \cos\theta} \left(J_1(\beta_\rho \rho) \sin^2 \varphi \;\; e^{j\beta\rho \sin\theta \cos\varphi} \; + \; J_1'(\beta_\rho \rho)\, \beta_\rho \rho \cos^2 \varphi \;\; e^{j\beta\rho \sin\theta \cos\varphi} \right) d\rho \, d\varphi$$

The integral equation presented above is solved using MATLAB.

Denominator of Eq. (4-21) can be split into two parts and can be calculated as,

$$D = \sqrt{D_1 * D_2}$$

where, $$D_1 = \iint |\boldsymbol{E_1}|^2 ds$$

and $$D_2 = \iint |\boldsymbol{E_2}|^2 ds$$

$$D_1 = \iint \left(\frac{J_1^2(\beta_\rho \rho)}{\rho^2} \sin^2 \varphi + J_1'^2(\beta_\rho \rho)\, \beta_\rho^2 \cos^2 \varphi \right) \rho d\rho \, d\varphi$$

The φ dependence in above integral can be solved directly because,

$$\int_0^{2\pi} \sin^2 \varphi \, d\varphi = \int_0^{2\pi} \cos^2 \varphi \, d\varphi = \pi$$

$$D_1 = \pi \int_0^a \left(\frac{J_1^2(\beta_\rho \rho)}{\rho} + J_1'^2(\beta_\rho \rho) \rho \beta_\rho^2 \right) d\rho$$

Using an identity of Bessel functions in order to simplify above equation we obtain,

$$D_1 = \pi \int_0^a \left(\frac{J_1^2(\beta_\rho \rho)}{\rho} + \left\{ J_0(\beta_\rho \rho) - \frac{J_1(\beta_\rho \rho)}{\beta_\rho \rho} \right\}^2 \rho \beta_\rho^2 \right) d\rho$$

$$= \pi \int_0^a \left(\frac{2J_1^2(\beta_\rho \rho)}{\rho} - 2J_0(\beta_\rho \rho)J_1(\beta_\rho \rho)\beta_\rho + J_0^2(\beta_\rho \rho)\rho\beta_\rho^2 \right) d\rho$$

Changing variable in order to simplify the integral further,

Let $$\beta_\rho \rho = x$$

$$\therefore \ \beta_\rho \, d\rho = dx$$

and changing the limits of integration accordingly, the integral becomes,

$$D_1 = \pi \int_0^{\beta_\rho a} \left(\frac{2J_1^2(x)}{x} - 2J_0(x)J_1(x) + xJ_0^2(x) \right) dx$$

For the dominant mode TE$_{11}$,

$$\beta_\rho a = \chi'_{11} = 1.841184$$

$$\therefore \ D_1 = 2\pi \int_0^{\chi'_{11}} \left\{ \frac{J_1^2(x)}{x} - J_0(x)J_1(x) + \frac{x}{2}J_0^2(x) \right\} dx$$

using MATLAB to evaluate the integral gives,

$$D_1 = 2\pi * 0.20225 = 1.27077 \ .$$

Consider the second term of the denominator,

$$D_2 = \iint (\sin^2 \varphi + \cos^2 \varphi) \, \rho d\rho \, d\varphi$$

$$D_2 = 2\pi \int_0^a \rho \, d\rho = \pi a^2 = 2.85023 \, x \, 10^{-6} \quad (\because a = 0.9525 \text{ mm})$$

The denominator D becomes,

$$D = 1.90315 \, x \, 10^{-3}$$

By using the value of N found using a MATLAB code and the above value of D, the coupling coefficient C is found for different values of incidence angles of the Gaussian beam. At $\theta = 0°$ and $45°$ of inclination of the Gaussian beam, the coupling coefficient C is 91.49% and 75.11% respectively.

This coupling hole model is simulated using CST Microwave Studio 2009. Simulation results are presented below. The structure and the dominant mode electric field distribution at the input of the iris are shown in Fig. 4-11.

Cut-off frequency for TE_{11} mode:- $f_c = 91.819$ GHz

The guided wavelength along the waveguide is calculated using,

$$\lambda_g = \frac{\lambda_0}{\sqrt{1-\left(\frac{f_c}{f}\right)^2}}$$

At $f = 110$ GHz, $\lambda_0 = 2.7273$ mm and for TE_{11} mode $f_c = 91.819$ GHz hence,

$$\lambda_g = 4.9526 \text{ mm}$$

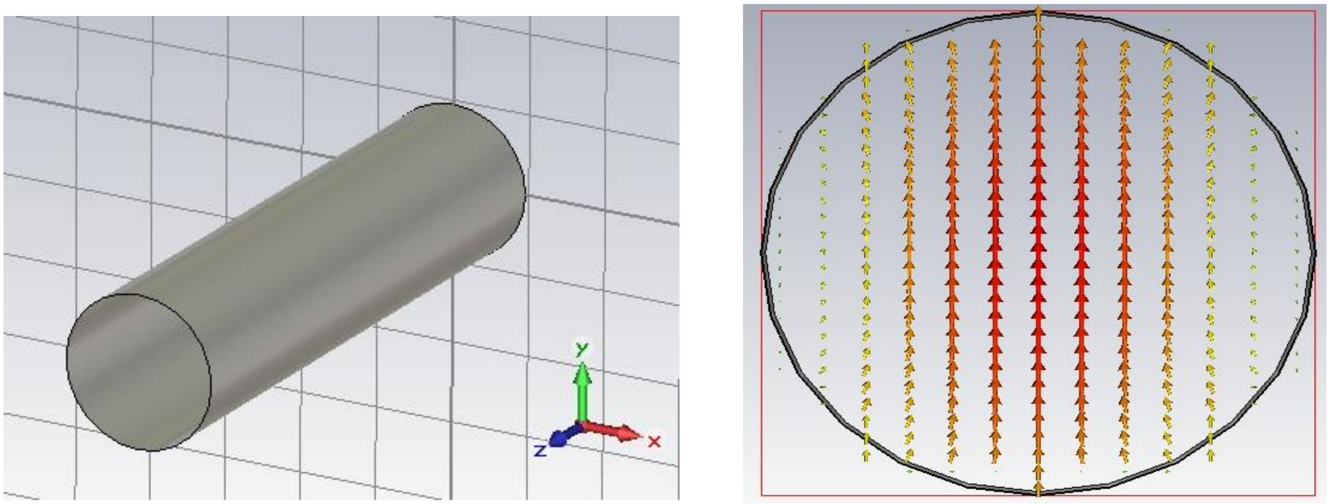

Fig. 4-11. Coupling hole and the dominant TE_{11} mode electric field distribution at the input of the iris.

The E-plane and H-plane radiation patterns of this simulated structure are shown in Fig. 4-12 and Fig. 4-13 respectively. The green circle in the radiation pattern figures represent the highest side lobe level, i.e the side lobe with maximum intensity out of all minor lobes located outside the main beam angular width. It is imperative to study the reflection coefficient as the amount of power we are dealing with is significantly high. The reflection coefficient seen at the input of coupling hole for a normal angle of incidence is plotted in Fig. 4-14. It is also a function of the length of the waveguide but for simple calculations the length of the waveguide is kept to be equal to 1.5λ_g, so that the magnitude of reflection is same at the end of the waveguide. It is observed that the reflection coefficient at 110 GHz is around 0.157 which is -16 dB.

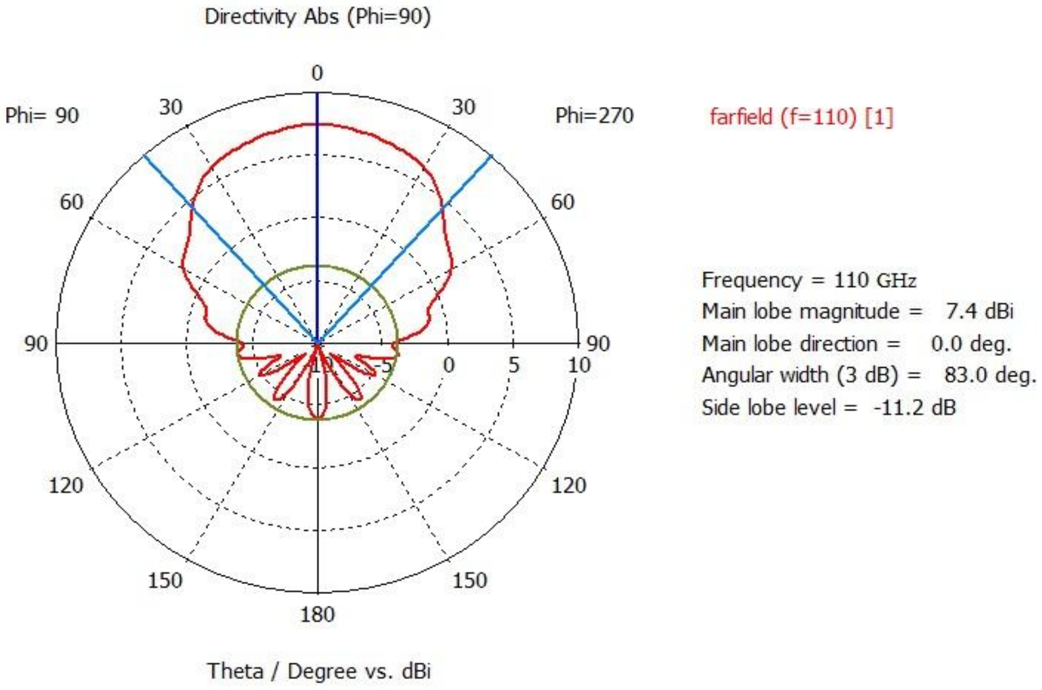

Fig. 4-12. E-plane radiation pattern of the coupling hole at 110 GHz.

APPLICATIONS

This resonator can be used to test the power handling capacity of waveguides, waveguide bends involving high power transmission over large distances.

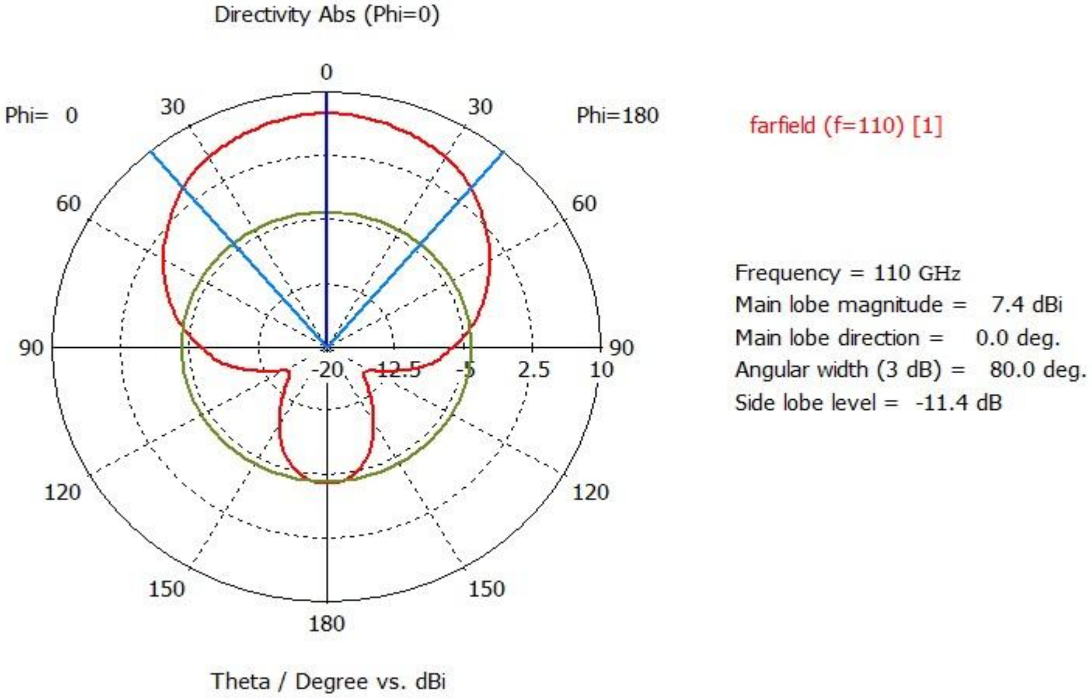

Fig. 4-13. H-plane radiation pattern of the coupling hole at 110 GHz.

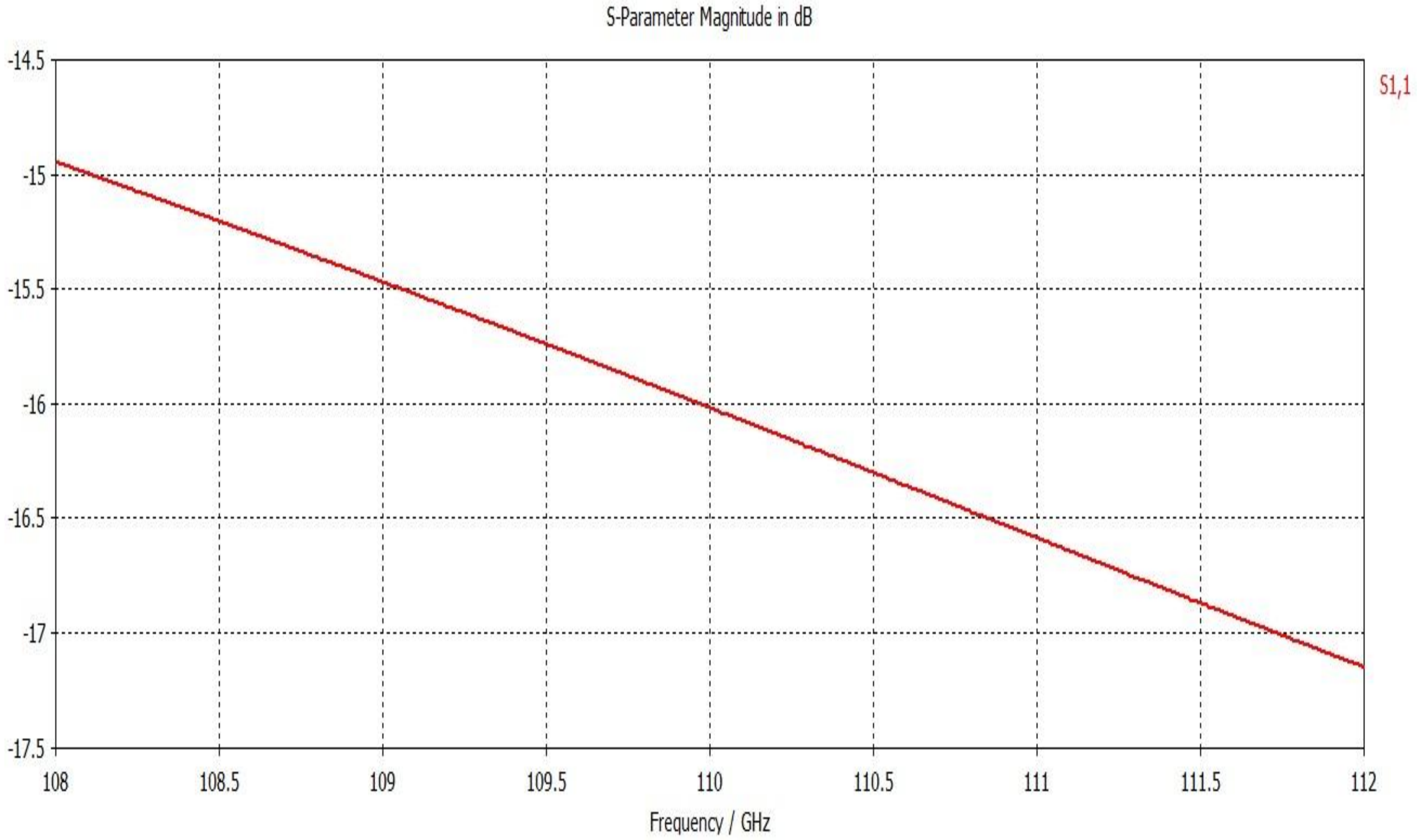

Fig. 4-14. Reflection Coefficient S_{11} (dB) of the coupling hole.

CONCLUSION

By knowing the waist diameter of the circulating mode, the coupling value for mode propagating in the coupling hole and the reflection coefficient, the power circulating inside the resonator can be found out.

REFERENCES

[1] Arthur D. Yaghjian, “Approximate Formulas for the Far Field and Gain of Open-ended Rectangular Waveguide,” *IEEE Trans. on Antennas and Propagation,* vol. AP-32, no. 4, pp. 378-384, April 1984.

[2] A. A. Bogdashov and G. G. Denisov, “Asymptotic Theory of High-efficiency Converters of Higher-order Modes into Eigenwaves of Open Mirror Lines,” *Radiophysics and Quantum Electronics,* vol. 47, no. 4, 2004.

[3] Samuel Silver, “Microwave Antenna Theory and Design,” *McGraw-Hill Book Co. Inc.*, 1949.

[4] Simon Ramo, John R. Whinnery, and Theodore Van Duzer, “Fields and Waves in Communication Electronics,” *3rd Edition,* John Wiley & Sons Inc., New York, 1994.

[5] H. Kogelnik, Appl. Opt. 4, 1562 (1965).

[6] L. J. Milosevic and R. Vautey, “Travelling Wave Resonator,” *IRE Transactions on Microwave Theory and Techniques*, vol. 6, pp. 136-143, April 1958.

[7] M. N. Afsar, Xiaohui Li and Hua Chi, “An Automated 60 GHz Open Resonator System for Precision Dielectric Measurement,” *IEEE Transactions on Microwave Theory and Techniques*, vol. 38, no.12, pp. 1845-1852, December 1990.

[8] C. A. Balanis, “Advanced Engineering Electromagnetics,” *John Wiley & Sons Inc.*, 1989.

[9] J. M. Moran, “Coupling of Power from a Confocal Laser with an Output Aperture,” *IEEE Journal of Quantum Electronics*, vol. QE-6, no. 2, February 1970.